LETTER TO THE EDITOR

Discovery of a dormant 33 solar-mass black hole in pre-release Gaia astrometry[⋆]

Gaia Collaboration: P. Panuzzo [1][⋆⋆], T. Mazeh [2], F. Arenou [1], B. Holl [3,4], E. Caffau [1], A. Jorissen [5], C. Babusiaux [6], P. Gavras [7], J. Sahlmann [7], U. Bastian [8], Ł. Wyrzykowski [9], L. Eyer [3], N. Leclerc [1], N. Bauchet [1], A. Bombrun [10], G.M. Seabroke [11], D. Teyssier [12], E. Balbinot [13,14], A. Helmi [13], A.G.A. Brown [14], A. Vallenari [15], T. Prusti [16], J.H.J. de Bruijne [16], A. Barbier [17], M. Biermann [8], O.L. Creevey [18], C. Ducourant [19], D.W. Evans [20], A. Hutton [21], C. Jordi [22,23], S.A. Klioner [24], U. Lammers [25], L. Lindegren [26], X. Luri [22,27,23], F. Mignard [18], P. Sartoretti [1], R. Smiljanic [28], P. Tanga [18], N.A. Walton [20], C. Aerts [29,30,31], C.A.L. Bailer-Jones [31], M. Cropper [11], R. Drimmel [32], F. Jansen [33], D. Katz [1], C. Soubiran [19], F. Thévenin [18], R. Andrae [31], M. Audard [3,4], J. Bakker [25], R. Blomme [34], J. Castañeda [35,22,23], F. De Angeli [20], C. Fabricius [23,22,27], M. Fouesneau [31], Y. Frémat [34], L. Galluccio [18], A. Guerrier [17], U. Heiter [36], E. Masana [23,22,27], F. Pailler [17], F. Riclet [17], W. Roux [17], G. Gracia-Abril [37,8], J. Portell [22,27,23], M. Altmann [8,38], K. Benson [11], J. Berthier [39], P.W. Burgess [20], D. Busonero [32], G. Busso [20], C. Cacciari [40], H. Cánovas [12], J.M. Carrasco [23,22,27], B. Carry [18], A. Cellino [32], N. Cheek [41], G. Clementini [40], Y. Damerdji [42,43], M. Davidson [44], P. de Teodoro [25], L. Delchambre [42], A. Dell'Oro [45], E. Fraile Garcia [7], D. Garabato [46], P. García-Lario [25], N.C. Hambly [44], D.L. Harrison [20,47], D. Hatzidimitriou [48], J. Hernández [25], D. Hestroffer [39], S. Jamal [31], G. Jevardat de Fombelle [3], S. Jordan [8], A. Krone-Martins [49,50], A.C. Lanzafame [51,52], W. Löffler [8], O. Marchal [53], A. Moitinho [50], K. Muinonen [54,55], M. Nuñez Campos [21], I. Oreshina-Slezak [18], P. Osborne [20], E. Pancino [45,56], T. Pauwels [34], A. Recio-Blanco [18], M. Riello [20], L. Rimoldini [4], A.C. Robin [57], T. Roegiers [58], L.M. Sarro [59], M. Schultheis [18], M. Smith [11], A. Sozzetti [32], E. Utrilla [21], M. van Leeuwen [20], K. Weingrill [60], U. Abbas [32], P. Ábrahám [61,62,63], A. Abreu Aramburu [64], S. Ahmed [20], G. Altavilla [65,56], M.A. Álvarez [46], F. Anders [22,27,23], E. Anglada Varela [21], T. Antoja [22,27,23], S. Baig [66], D. Baines [67], S.G. Baker [11], L. Balaguer-Núñez [23,22,27], Z. Balog [8,31], C. Barache [38], M. Barros [68], M.A. Barstow [69], D. Bashi [2,70], N. Baudeau [71], L.R. Bedin [15], M. Bellazzini [40], W. Beordo [32,72], M. Bernet [22,27,23], C. Bertolotto [73], S. Bertone [32,74], L. Bianchi [75], A. Binnenfeld [76], S. Blanco-Cuaresma [77,78], J. Bland-Hawthorn [79,80], A. Blazere [81], T. Boch [53], D. Bossini [82,15], S. Bouquillon [38,83], A. Bragaglia [40], E. Bratsolis [84], E. Breedt [20], A. Bressan [85], N. Brouillet [19], E. Brugaletta [51], B. Bucciarelli [32,72], A.G. Butkevich [32], A. Camut [86], R. Cancelliere [87], T. Cantat-Gaudin [31], D. Capilla Guilarte [20], R. Carballo [88], T. Carlucci [38], M.I. Carnerero [32], J. Carretero [89,90,91], S. Carton [92], L. Casamiquela [1], M. Castellani [65], A. Castro-Ginard [14], V. Cesare [51], P. Charlot [19], C. Chaudet [4], L. Chemin [93], A. Chiavassa [18], N. Chornay [4], D. Chosson [94], W.J. Cooper [66,32], M. Crosta [32,95], C. Crowley [10], M. Cruz Reyes [96], C. Dafonte [46], M. Dal Ponte [15], M. David [97], P. de Laverny [18], F. De Luise [98], R. De March [73], J. De Ridder [29], A. de Torres [10], E.F. del Peloso [8], A. Delgado [7], J.-B. Delisle [3], C. Demouchy [99], E. Denis [18,100], T.E. Dharmawardena [101,102], F. Di Giacomo [98], C. Diener [20], C. Dolding [11], K. Dsilva [5], C. Fabre [81], M. Fabrizio [65,56], S. Faigler [2], M. Fatović [103], G. Fedorets [104,54,105], J. Fernández-Hernández [7], P. Fernique [53], F. Figueras [22,27,23], C. Fouron [71], F. Fragkoudi [106], M. Gai [32], M. Galinier [18], A. Garcia-Serrano [23,22,27], M. García-Torres [107], A. Garofalo [40], E. Gerlach [24], R. Geyer [24], P. Giacobbe [32], G. Gilmore [20,108], S. Girona [109], G. Giuffrida [65], A. Gomboc [110], A. Gomez [46], I. González-Santamaría [46], E. Gosset [42,111], M. Granvik [54,112], V. Gregori Barrera [23,22,27], R. Gutiérrez-Sánchez [12], M. Haywood [1], A. Helmer [92], T. Hilger [24], D. Hobbs [26], C. Hottier [1], H.E. Huckle [11], Ó. Jiménez-Arranz [22,27,23], J. Juaristi Campillo [8], Z. Kaczmarek [8], P. Kervella [94], S. Khanna [32,13], G. Kordopatis [18], A.J. Korn [36], Á Kóspál [61,31,62], Z. Kostrzewa-Rutkowska [64,14], K. Kruszyńska [113], M. Kun [61], S. Lambert [38], Y. Lebreton [94,114], T. Lebzelter [63], S. Leccia [115], G. Lecoutre [57], S. Liao [116,32,117], L. Liberato [18,118], E. Licata [32], E. Livanou [48], J. López-Miralles [21], M. Madarász [61], L. Mahy [34], R.G. Mann [44], M. Manteiga [119], C.P. Marcellino [51], J.M. Marchant [120], M. Marconi [115], D. Marín Pina [22,27,23], S. Marinoni [65,56], D.J. Marshall [121], J. Martín Lozano [41], L. Martin Polo [122], G. Marton [61], D. Mascarenhas [92], A. Masip [23,22,27], A. Mastrobuono-Battisti [1], P.J. McMillan [69], J. Meichsner [24], J. Merc [123], S. Messina [51], N.R. Millar [20], A. Mints [60], D. Mohamed [86], D. Molina [27,22,23], M. Monguió [22,124], P. Montegriffo [40], L. Monti [40], A. Mora [21], R. Morbidelli [32], D. Morris [44], R. Mudimadugula [60], T. Muraveva

[40], I. Musella [115], Z. Nagy [61], N. Nardetto [18], C. Navarrete [18], S. Oh [20, 125], C. Ordenovic[18], O. Orenstein [2], C. Pagani [69], I. Pagano [51], L. Palaversa [103], P.A. Palicio [18], L. Pallas-Quintela [46], M. Pawlak [126, 26], A. Penttilä [54], P. Pesciullesi[7], M. Pinamonti [32], E. Plachy [61, 62], L. Planquart [5], G. Plum[1], E. Poggio [32, 18], D. Pourbaix† [5, 111], A. Price-Whelan [127], V. Rabin[39], M. Rainer [128, 45], C.M. Raiteri [32], P. Ramos [129, 22, 23], M. Ramos-Lerate [12], M. Ratajczak [9], P. Re Fiorentin [32], S. Regibo [29], C. Reylé [57], V. Ripepi [115], A. Riva [32], H.-W. Rix [31], G. Rixon [20], G. Robert[92], N. Robichon [1], C. Robin[92], M. Romero-Gómez [22, 27, 23], N. Rowell [44], D. Ruz Mieres [20], G. Sadowski [5], A. Sagristà Sellés [8], N. Sanna [45], C. Sarrate Riera[35, 22, 23], E. Sciacca [51], D. Ségransan [3], S. Shahaf [130], A. Siebert [53, 131], E. Slezak[18], R.L. Smart [32, 66], O.N. Snaith [1, 132], E. Solano [133], F. Solitro[73], D. Souami [94, 134], J. Souchay[38], E. Spitoni [18, 135], F. Spoto [77], I.A. Steele [120], J. Surdej [42], L. Szabados [61], F. Taris[38], M.B. Taylor [136], R. Teixeira [137], T. Tepper-Garcia [79, 80], W. Thuillot [39], N. Tonello [109], F. Torra [22, 27, 23], G. Torralba Elipe [46, 138, 139], M. Trabucchi [82, 3], E. Trentin [140, 115], M. Tsantaki [45], C. Turon [1], A. Ulla [141, 142], N. Unger [3], I. Valtchanov [12], O. Vanel [1], A. Vecchiato [32], D. Vicente [109], E. Villar[35, 22, 23], H. Zhao [18, 143], J. Zorec [144], S. Zucker [76, 2], A. Župić [46], and T. Zwitter [145]

(Affiliations can be found after the references)

ABSTRACT

Context. Gravitational waves from black-hole (BH) merging events have revealed a population of extra-galactic BHs residing in short-period binaries with masses that are higher than expected based on most stellar evolution models – and also higher than known stellar-origin black holes in our Galaxy. It has been proposed that those high-mass BHs are the remnants of massive metal-poor stars.

Aims. *Gaia* astrometry is expected to uncover many Galactic wide-binary systems containing dormant BHs, which may not have been detected before. The study of this population will provide new information on the BH-mass distribution in binaries and shed light on their formation mechanisms and progenitors.

Methods. As part of the validation efforts in preparation for the fourth *Gaia* data release (DR4), we analysed the preliminary astrometric binary solutions, obtained by the *Gaia* Non-Single Star pipeline, to verify their significance and to minimise false-detection rates in high-mass-function orbital solutions.

Results. The astrometric binary solution of one source, *Gaia* BH3, implies the presence of a 32.70 ± 0.82 $M_\odot$ BH in a binary system with a period of 11.6 yr. *Gaia* radial velocities independently validate the astrometric orbit. Broad-band photometric and spectroscopic data show that the visible component is an old, very metal-poor giant of the Galactic halo, at a distance of 590 pc.

Conclusions. The BH in the *Gaia* BH3 system is more massive than any other Galactic stellar-origin BH known thus far. The low metallicity of the star companion supports the scenario that metal-poor massive stars are progenitors of the high-mass BHs detected by gravitational-wave telescopes. The Galactic orbit of the system and its metallicity indicate that it might belong to the Sequoia halo substructure. Alternatively, and more plausibly, it could belong to the ED-2 stream, which likely originated from a globular cluster that had been disrupted by the Milky Way.

Key words. astrometry – binaries: spectroscopic – Stars: evolution – Stars: massive – Stars: black holes – Stars: Population II

1. Introduction

Since the first event detected in 2015 (Abbott et al. 2016) by the LIGO/Virgo collaboration, the detection of black-hole (BH) mergers via gravitational waves has uncovered the existence of a population of BHs residing in short-period binaries with masses higher than $30 M_\odot$, ranging up to $85 M_\odot$ (Abbott et al. 2020, 2021).

Stellar evolution models have difficulties in explaining such large masses for BHs of stellar origin: stars with an initial mass larger than $30 M_\odot$ are predicted to lose most of their mass during their evolution, due to the onset of strong winds, producing BHs with masses below $20 M_\odot$ (Vink 2008; Belczynski et al. 2007; Sukhbold et al. 2016).

The masses of the merging BHs detected via gravitational waves are also larger than any known stellar-origin BHs in our Galaxy: all confirmed or candidate BHs of stellar origin in the Milky Way have typical masses around or below $10 M_\odot$, with

Cyg X-1 ($\sim 20 M_\odot$, Miller-Jones et al. 2021) being the most massive one known thus far. However, the known stellar-origin BHs, mainly limited to short-period X-ray binaries, are only a very tiny fraction of the expected number of BHs in our Galaxy ($\sim 10^8$ e.g. Olejak et al. 2020). In fact, stellar-origin BHs are hard to detect because most of them do not interact with a companion. So, the lack of data on BHs with masses larger than $20 M_\odot$ could be due to an observational bias. Indirect methods such as gravitational microlensing have also yielded only one robust discovery of a single BH with mass, of about $7 M_\odot$ (Sahu et al. 2022).

The detection of mergers of BHs with masses larger than $30 M_\odot$ can be reconciled with stellar evolution models if the progenitors of the high-mass BHs are low-metallicity stars (Belczynski et al. 2010a, 2016; Fryer et al. 2012). The lack of metals substantially decreases the mass loss during the stellar lifetime (Vink 2008) and reduces the radius of the evolving progenitors (Hurley et al. 2000; Belczynski et al. 2010a), the latter effect decreasing the probability of merging during the common-envelope phase (Belczynski et al. 2007) in binary systems. Finally, the higher mass of the BHs produced by low-metallicity progenitors is expected to decrease substantially or eliminate the natal kick strength at the birth of the BHs, preserving the binary as a bound system (Belczynski et al. 2010b). The maximum

---

metallicity for the formation of the high-mass BHs is a matter of active debate, with some models predicting the formation of 30 $M_\odot$ BHs even at solar metallicities (Bavera et al. 2023).

Since its Data Release 3 (DR3, Gaia Collaboration et al. 2023b), the *Gaia* mission (Gaia Collaboration et al. 2016) has increased the number of detected stellar binary systems by two orders of magnitude (Gaia Collaboration et al. 2023a; Halbwachs et al. 2023, Gosset et al. in prep.). This has opened up the possibility of detecting BHs in binary systems that do not interact with their companion. Moreover, the ability of *Gaia* to measure the astrometric orbit of such systems allows the measurement of the inclination of the orbit, providing a robust estimate of the mass of the dark companion. Two dormant BHs, *Gaia* BH1 and BH2 (El-Badry et al. 2023a,b; Tanikawa et al. 2023; Chakrabarti et al. 2023) were discovered in *Gaia* binaries of DR3. *Gaia* Data Release 4 (DR4) is expected to contain a larger number of binary systems than *Gaia* DR3; consequently, this will provide a greater number of BH-hosting systems, which will help to shed light on the BH population and the mechanisms in action in the BHs' formation.

In this Letter, we report the serendipitous discovery of a nearby (∼590 pc) binary system composed of an old, very metal-poor,[1] giant star orbiting a BH in 11.6 yr. The estimated BH mass, 33 $M_\odot$, is substantially higher than all known Galactic BHs and is in the mass range of the extra-galactic BHs detected by gravitational waves.

The system was identified while validating the preliminary *Gaia* astrometric binary solutions produced in preparation for DR4 and subsequently confirmed by *Gaia* RVS radial-velocity data. We took the exceptional step of the publication of this paper based on preliminary data ahead of the official DR4 due to the unique nature of the discovery, which we believe should not be kept from the scientific community until the next release. An early disclosure will also enable an early and extensive follow-up by the community.

2. Observations and analysis

2.1. Properties of the source

Gaia DR3 4318465066420528000 (also known as LS II +14 13 and 2MASS J19391872+1455542), hereafter denoted as *Gaia* BH3, is a bright source in the constellation Aquila, known to be a high proper-motion star (Lépine & Shara 2005). Its basic properties from the *Gaia* DR3 archive are reported in Table 1. Its absolute magnitude and color (Riello et al. 2021; Sartoretti et al. 2023) identify it as a star climbing the giant branch (see Fig. 1). The source was analysed by the Astrophysical Parameters Inference System (Apsis, Creevey et al. 2023; Fouesneau et al. 2023). It has been identified as a G spectral-type star by the ESP-ELS algorithm (Sect 11.3.7 of the online documentation, Ulla et al. 2022) and the GSP-Spec ANN parameters (Recio-Blanco et al. 2023) indicate it as a metal-poor giant. No GSP-Phot result (Andrae et al. 2023) is published in the *Gaia* archive, while the parameters provided by GSP-Spec MatisseGauguin (Recio-Blanco et al. 2023) carry large uncertainties.

The source is not known as a variable star in the literature, neither in the AAVSO International Database, nor in the ASAS-SN database. We inspected ASAS-SN, ZTF, and TESS photometry, finding that the source does not present any significant periodic variability. The source was not observed with

---

[1] We use the nomenclature from Beers & Christlieb (2005) where very metal-poor are those stars having [Fe/H] < −2.

Table 1. Basic properties of *Gaia* BH3 from the *Gaia* DR3 catalogue. Astrophysical parameters are from GSP-Spec ANN.

Parameter	Value
α [deg]	294.8278625082[a]
σ_{α^*} [mas]	0.051
δ [deg]	14.9309796086[a]
σ_δ [mas]	0.052
ϖ [mas]	1.679 ± 0.069[b]
μ_α^* [mas yr^{-1}]	−22.235 ± 0.062
μ_δ [mas yr^{-1}]	−155.276 ± 0.059
G [mag]	11.2311 ± 0.0028
$G_{BP} - G_{RP}$ [mag]	1.2156 ± 0.0048
G_{RVS} [mag]	10.2289 ± 0.0122
T_{eff} [K]	5340^{+212}_{-198}
$\log g$	$3.08^{+0.36}_{-0.30}$
[M/H]	$-2.76^{+0.19}_{-0.09}$
[α/Fe]	0.54 ± 0.06
RV [km s^{-1}]	−333.2 ± 3.4

Notes. [a] The reference epoch of DR3 coordinates is J2016.0 (JD 2457389.0). [b] A zero-point correction (Lindegren et al. 2021a) of 35.4 μas has been applied to the parallax value given in the catalogue.
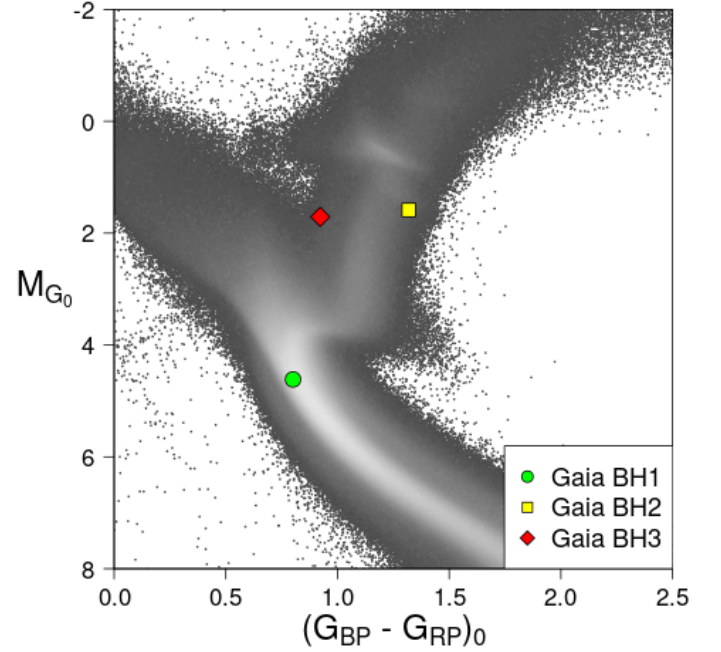

Fig. 1. *Gaia* BH3 position in the *Gaia* color-magnitude diagram, compared with the position of Gaia BH1, BH2 and the low extinction ($A_0 < 0.05$ mag) *Gaia* DR3 color-magnitude diagram. All extinctions are estimated through the Lallement et al. (2022) extinction map.

XMM-Newton, Chandra nor GALEX, nor it is present in the RAVE, APOGEE, LAMOST, or GALAH spectroscopic surveys. No eROSITA data have been made available yet for *Gaia* BH3, which belongs to the eastern Galactic hemisphere.

2.2. Astrometry and orbital solution

The system was identified while validating astrometric binaries orbital solutions produced by the Non-Single Star (NSS) pipeline in a preliminary run (identified as NSS 4.1), done in
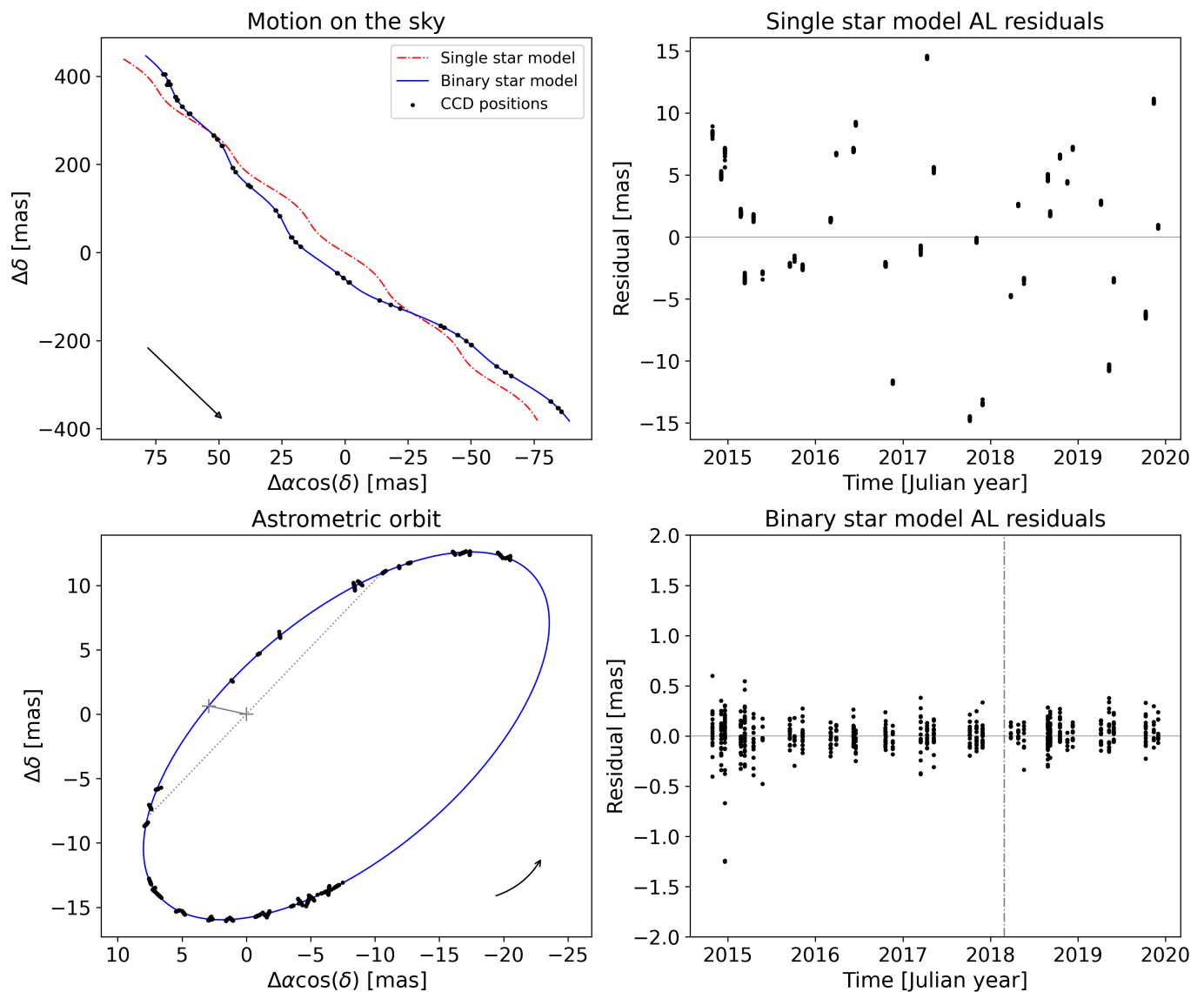
Fig. 2. Astrometric data of *Gaia* BH3. Top-left panel: Motion on the sky of the photocentre of the source, as seen by *Gaia* in the different CCD transits (dots), compared with the best fitting single-star solution from AGIS and the astrometric-binary solution from the NSS pipeline; the arrow indicates the direction of the proper motion. Bottom-left panel: Derived astrometric orbit of the photocentre, after a subtraction of parallax and proper motion, compared with the astrometric measurements. We note that only one-dimensional (1D) along-scan (AL) astrometry was used by the NSS pipeline. The position of the photocentre on the sky corresponding to each measurement is derived combining the measured one-dimensional AL position and the assumed orbital solution. The + signs show the barycentre and the position of the periastron, the dotted line shows the line of nodes, and the arrow indicates the direction of the motion along the orbit. In the top-right and bottom-right panels, we can see the residuals of the along-scan (AL) astrometric measurements for, respectively, the single-star solution and the binary-star solution. The vertical dot-dashed line in the bottom-right panel marks the time of the periastron passage.

preparation of *Gaia* DR4. The NSS pipeline used in the NSS 4.1 run is similar to the one used in the *Gaia* DR3, which is described in Halbwachs et al. (2023) and in Section 7.2.2 of the DR3 NSS documentation (Pourbaix et al. 2022), with improvements in the filtering of spurious solutions. The NSS pipeline processed astrometric data produced by preliminary runs of the Intermediate Data Update (IDU; see Fabricius et al. 2016) and the Astrometric Global Iterative Solution (AGIS; see Lindegren et al. 2021b) pipelines, covering the time range from JD 2456941.6218 to JD 2458869.4177 (TCB[2]), for a total of about 64 months. The NSS 4.1 run was executed on an input list of 10.4 million sources,

chosen to be brighter than $G_{RVS} = 14$ mag, and produced almost 1.5 million orbital solutions. We note that the final NSS run for DR4 will extend to fainter magnitudes, and it is expected to produce a much larger number of binary solutions. Further details on the NSS 4.1 run can be found in Appendix A.

For each orbital solution, we computed the astrometric mass function from the angular semi-major axis of the photocentre orbit (a_0), period (P), and parallax (ϖ) as:

$$f_M = (a_0/\varpi)^3 (1 \, \text{yr}/P)^2 \, M_\odot . \tag{1}$$

For an astrometric binary, the mass function depends on the masses of the components (M_1, M_2) and on their flux ratio, $\mathcal{F}_2/\mathcal{F}_1$ (Halbwachs et al. 2023). For an invisible companion

---

[2] TCB: Barycentric Coordinate Time, the time scale used here for all *Gaia* dates.

Table 2. Campbell orbital elements of the *Gaia* BH3 system and the astrometric parameters of its barycentre.

Parameter	Astrometric solution	Combined solution
α [deg]	294.8278502411[a]	294.8278502301[a]
$\sigma_{\alpha*}$ [mas]	0.060	0.054
δ [deg]	14.9309190720[a]	14.9309190869[a]
σ_δ [mas]	0.086	0.074
ϖ [mas]	1.6747 ± 0.0094	1.6933 ± 0.0164[b]
μ_α^* [mas yr^{-1}]	-28.372 ± 0.077	-28.317 ± 0.067
μ_δ [mas yr^{-1}]	-155.150 ± 0.129	-155.221 ± 0.111
P [days]	4194.7 ± 112.3	4253.1 ± 98.5
e	0.7262 ± 0.0056	0.7291 ± 0.0048
a_0 [mas]	27.07 ± 0.56	27.39 ± 0.49
i [deg]	110.659 ± 0.107	110.580 ± 0.095
T_p [JD, TCB]	2458177.28 ± 0.98	2458177.39 ± 0.88
Ω [deg]	136.200 ± 0.147	136.236 ± 0.128
ω [deg]	77.77 ± 0.66	77.34 ± 0.76
a_1 [AU]	...	16.17 ± 0.27
γ [km s^{-1}]	...	-357.31 ± 0.44
f_M [$M_\odot$]	32.03 ± 0.64	31.23 ± 0.81
GoF	2.17	-0.53

Notes. [a] The reference epoch of DR4 coordinates is J2017.5 (JD 2457936.875). [b] Derived as a_0/a_1, see text.

$(\mathcal{F}_2/\mathcal{F}_1 = 0)$ the mass function simplifies to:

$$f_M = M_2 \left(\frac{M_2}{M_1 + M_2} \right)^2 , \qquad (2)$$

from which it follows that $M_2 \geq f_M$. Given f_M and an estimate of the mass of the visible component (M_1), Eq. (2) can be used to solve for the mass of the dark companion (M_2).

Among the 1.5 million orbital solutions, *Gaia* BH3 yielded the largest mass function, $32.03 \pm 0.64\,M_\odot$, with a significance (a_0/σ_{a_0}) of 48.1; no other solution has a mass function larger than $20\,M_\odot$. In Fig. 2, we show the orbital solution and the residuals, from which the strength of the astrometric signal of the orbit, along with the the robustness and quality of the solution can be appreciated. The Campbell orbital elements of the source are reported in the central column of Table 2. We note that the NSS pipeline used in this preliminary run produces Thiele-Innes elements; the Campbell elements and their uncertainties were computed using the equations in Appendix A of Halbwachs et al. (2023). The astrometric mass function value and its uncertainty were computed using Monte Carlo resampling of the Thiele-Innes elements, the parallax and the period, in order to take into account the correlations between parameters; in particular, between a_0 and the period. To make sure this procedure would yield reliable results, we first checked that the correlations are sufficiently well behaved to allow for Monte Carlo resampling, following Section 6.1 of Babusiaux et al. (2023).

A word of caution is necessary on the parallax value, and thus on the astrometric mass function: as in previous releases, the *Gaia* parallaxes are affected by a small bias (see Lindegren et al. 2021a), but we do not have enough information at this stage to quantify the bias for the preliminary NSS solutions. As a consequence, the uncertainty on the mass function reported in Table 2 is underestimated.
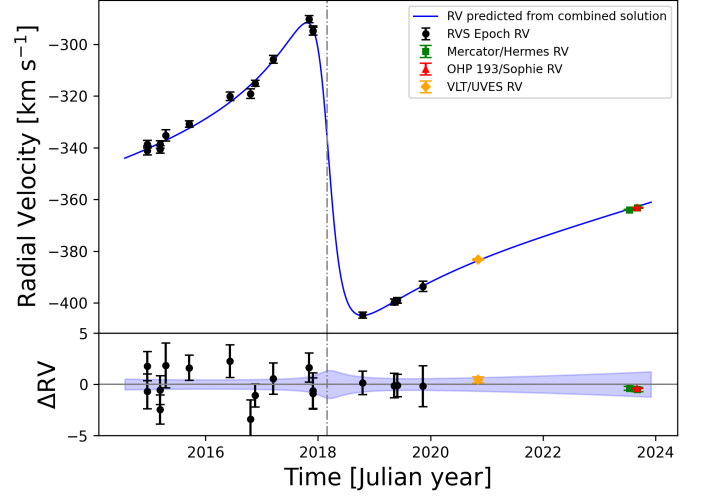

Fig. 3. Radial-velocity evolution of *Gaia* BH3. Top panel: Comparison between the radial-velocity evolution predicted from the combined *Gaia* astrometric-spectroscopic binary model (blue solid line) and the epoch radial velocities measured with the *Gaia* RVS instrument (black filled circles), and ground-based measurements for *Gaia* BH3. Bottom panel: Radial-velocity residuals with respect to the binary solution compared with the 1-σ uncertainty of the predicted radial-velocity evolution (blue shaded area). The vertical dot-dashed line in both panels marks the time of the periastron passage.
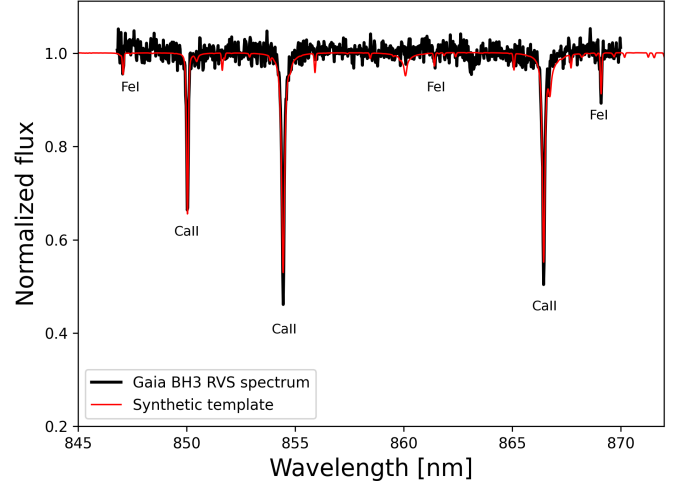

Fig. 4. *Gaia* RVS combined spectrum of *Gaia* BH3, in restframe, compared with the template spectrum.

2.3. Spectroscopy and combined orbital solution

The *Gaia* RVS (Cropper et al. 2018) data of sources with an orbital solution from the NSS 4.1 run were processed with the DR4 operational RVS pipeline. Improvements with respect to the DR3 version will be described in the *Gaia* DR4 documentation; the DR3 RVS pipeline is described in Sartoretti et al. (2018), Katz et al. (2023), and Sartoretti et al. (2022). It is worth mentioning that the DR4 RVS pipeline includes the correction for the effect of the astrometric orbital motion, discussed in Holl et al. (2023); in particular, Section 3.3.1. The DR4 RVS data cover the time range from JD 2456863.9385 to JD 2458869.4177, namely, about 67 months. The pipeline produced 17 valid epoch radial velocities for *Gaia* BH3, reported in Appendix B, using a template spectrum with $T_{\rm eff} = 6000\,{\rm K}$, $\log g = 3.5$ and

[Fe/H] = −1.5 (see Blomme et al. 2017). The template parameters were estimated by the pipeline from the RVS spectrum itself.

We used the DR3 NSS pipeline code to compute an orbital solution combining astrometric data and *Gaia* RVS radial velocities (nss_solution_type = AstroSpectroSB1). The details of the adopted model are described in Section 7.7.3 of Pourbaix et al. (2022). We recall that in the combined solution model only the period, eccentricity, and periastron time are in common between the astrometric and the spectroscopic part of the solution. There is no constraint to impose that the semi-major axis of the photocentre orbit in AU (= a_0/ϖ) would be equal to the semi-major axis of the spectroscopic orbit a_1, as expected in the case of a dark companion. The consistency between a_0 and a_1 allows us to check whether the flux ratio is indeed compatible with a value of zero.

As discussed in Sect. 2.2, the parallax derived by the NSS pipeline for the combined solution ($\varpi = 1.6808 \pm 0.0086\,\text{mas}$) is affected by a bias which we cannot quantify. In order to avoid its effect on the mass function, we estimate the latter using a_1 instead of a_0/ϖ, namely:

$$f_M = \left(\frac{a_1}{1\,\text{AU}}\right)^3 \left(\frac{1\,\text{yr}}{P}\right)^2 M_\odot , \qquad (3)$$

resulting in a value of $31.23 \pm 0.81\,M_\odot$. Assuming the equality between the photocentre and the spectroscopic orbit, we can also provide an alternative estimation of the parallax as

$$\varpi = a_0/a_1 , \qquad (4)$$

which results in a value of $1.6933 \pm 0.0164\,\text{mas}$.

The Campbell orbital elements of the combined solution for *Gaia* BH3 are reported in Table 2. The combined solution is very similar to the astrometric solution, with slightly smaller uncertainties, and a better goodness-of-fit (GoF, in the Hipparcos sense, see Pourbaix et al. 2022), as a result of a stronger filtering of outliers. Radial velocities predicted by the combined solution are compared with the measurements in Fig. 3. In Fig. 4, we show the combined and normalised RVS spectrum (see Seabroke et al. in prep.) compared with the template spectrum.

Given the extreme value of the mass function of the system and the importance of its detection, a confirmation with ground-based observations was indispensable to discard the possibility of a spurious solution. We thus observed *Gaia* BH3 with the HERMES spectrograph (Raskin et al. 2011) mounted on the 1.2-meter Mercator telescope at the Roque de los Muchachos Observatory (Spain), and with the SOPHIE spectrograph (Perruchot et al. 2008) mounted on the 1.93-meter telescope of the Observatoire de Haute-Provence (France). A search in the ESO archive revealed that the source was observed with the UVES spectrograph (Dekker et al. 2000) mounted on the VLT. Details on the data reduction of these observations can be found in Appendix C. The spectra do not show any sign of the presence of a second component, nor of continuum filling of absorption lines; furthermore, no emission line was detected. Radial velocities were derived for each ground-based observation and their values are reported in Table C.1. Although these values were not used to derive the orbital solution described above, they are in agreement with the predicted radial velocity within 0.5 km s^{-1}; this is less than the uncertainty of the orbital solution, as can be seen in Fig. 3. This result confirms the reality and accuracy of the orbital solution derived from *Gaia* data.

Table 3. Stellar parameters of *Gaia* BH3 derived in this work.

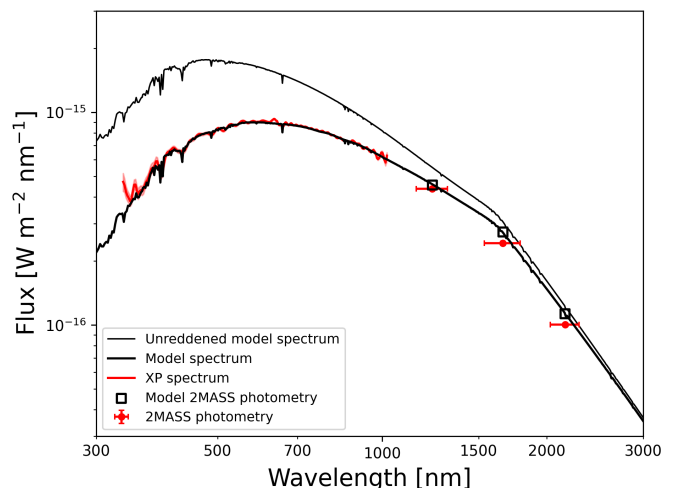| Parameter	Value
T_{eff} [K]	5212 ± 80
$\log g$	2.929 ± 0.003
[Fe/H]	-2.56 ± 0.11
[α/Fe]	0.43 ± 0.12
[M/H]	-2.21 ± 0.15
$\log(L_\star/L_\odot)$	1.208 ± 0.030
$M_\star$ [$M_\odot$]	0.76 ± 0.05
$R_\star$ [$R_\odot$]	4.936 ± 0.016
$M_{\text{G},0}$ [mag]	1.778 ± 0.082
$(G_{\text{BP}} - G_{\text{RP}})_0$ [mag]	0.921 ± 0.031

Fig. 5. *Gaia* BH3 modelled SED, compared with the *Gaia* XP spectrum and 2MASS photometry. The thin black line shows the unreddened model, while the thick line shows the SED assuming $A_0 = 0.71$ mag.

2.4. Stellar parameters, abundances and Galactic orbit

We derived new stellar parameters of the luminous component, using the *Gaia* DR3 photometry (G magnitude and $G_{\text{BP}} - G_{\text{RP}}$ colour), the parallax from the combined astrometric-spectroscopic solution, and the extinction (A_0) derived from the dust extinction maps of Vergely et al. (2022), with an iterative procedure described in Appendix D. The UVES spectrum was used to determine the metallicity and abundances (see Appendix E). We then compared the extinction-corrected absolute G magnitude ($M_{\text{G},0}$) and the dereddened colour $(G_{\text{BP}} - G_{\text{RP}})_0$ with the ones given by the isochrones libraries PARSEC (Bressan et al. 2012) and BaSTI (Pietrinferni et al. 2021). Thus, we derived the mass ($M_\star$) of the visible component. The parameters are reported in Table 3.

In Fig. 5, we compare the expected spectral energy distribution (SED) with the *Gaia* XP spectrum (Carrasco et al. 2021; De Angeli et al. 2023; Montegriffo et al. 2023) and 2MASS photometry. The agreement between the predicted SED and the *Gaia* XP spectrum is very good, with the only exception of the blue edge, where the XP spectrum is noisier.

The abundances of *Gaia* BH3 (reported in Appendix E) show that the star is α-enhanced, as expected for a very metal-poor star. There is no trace of ^{13}C in the spectrum and the [Ba/Fe] is nearly solar, indicating the star has not been enriched by material processed in the CNO cycle, as expected if it had, for instance, accreted material from a companion star in the AGB

phase. The star has no chemical peculiarity, except an enhancement of Eu ([Eu/Fe] = 0.52). Thus, it can be classified as an r-I neutron-capture-rich star, following the classification of Beers & Christlieb (2005).

Using the systemic radial velocity, proper motion, position, and distance, and assuming the Milky Way gravitational potential from McMillan (2017), we may find that the source has a high-energy retrograde orbit[3] ($E = -1.29 \times 10^5$ km^2 s^{-2}, $L_z = -2.3 \times 10^3$ kpc km s^{-1}, $L_\perp = 1.05 \times 10^3$ kpc km s^{-1}) in the Galaxy. Its kinematic characteristics are consistent with those of the halo substructure known as Sequoia (Myeong et al. 2019), but are also in agreement to those of the recently discovered ED-2 stream (Dodd et al. 2023; Balbinot et al. 2023), a likely remnant of a globular cluster that was disrupted by the Milky Way. The metallicity of *Gaia* BH3 is more consistent with ED-2 ([Fe/H] = -2.6 ± 0.2) than with the median metallicity of Sequoia ([Fe/H] ~ -1.7).

3. Discussion

With an estimated mass of $0.76 \pm 0.05\ M_\odot$ for the luminous companion, we derived a mass of:

$$M_{\mathrm{BH}} = 32.70 \pm 0.82\ M_\odot \,, \tag{5}$$

for the dark companion. The observed luminosity of *Gaia* BH3 is too low by several orders of magnitude to be compatible with the hypothesis that the companion is a main sequence star or even two main sequence stars in a close orbit. The estimated mass is also too large for one neutron star or two neutron stars in a close orbit, so we are left with the possibility of: 1) a single BH; 2) an inner binary containing two BHs; or 3) a BH and another compact object. Although the single BH is the simplest explanation, the hypothesis of an inner binary of two BHs cannot be excluded. Hayashi et al. (2023) proposed a method to test this hypothesis by detecting radial-velocity perturbations at the periastron. Using the Hayashi et al. (2023) formulation, we estimated radial-velocity perturbations[4] with a maximum amplitude of the order of 0.2 km s^{-1}. Such perturbations are too small to be detected in the *Gaia* RVS data, but can be verified with ground-based instruments (see Nagarajan et al. 2024, for an application to *Gaia* BH1). For the purposes of the subsequent discussion, we have adopted the single BH hypothesis as the most likely explanation.

The estimated mass of the BH in *Gaia* BH3 makes it the most massive BH of stellar origin discovered in our Galaxy. It is striking that the only BH with a mass larger than $20\ M_\odot$ found in the *Gaia* data so far is in orbit with a very metal-poor star, while such stars make up only a tiny fraction of the stars analysed in the NSS pipeline run (0.4% of sources which produced a binary solution have [M/H] < -2 from DR3 GSP-Phot). Such stars also make up a small fraction of our Galactic halo (less than 5% according to Bonifacio et al. 2021) where this star and the majority of metal-poor stars are located. Although we can not exclude that this BH is the result of the merger of two less massive BHs, this discovery strongly supports the scenario where high-mass BHs are remnants of low-metallicity stars. The above considerations also raise the question of the maximum metallicity value for the

---

[3] Here we use the same conventions as in Myeong et al. (2019).
[4] We use $K_{\mathrm{short}}(1-e)^{-7/2}$ as perturbations level estimation, (see Sect. 2.1 in Hayashi et al. 2023), assuming an inner equal-mass binary with a circular coplanar orbit, and a period corresponding to the maximum allowed by dynamic stability (126 days, according to eq. 6 in Hayashi et al. 2023).

formation of high-mass BHs, which in Belczynski et al. (2016) is identified at [M/H] = -1. The much lower metallicity of *Gaia* BH3 may be an indication that high-mass BHs form only at very low metallicities rather than at moderately low ones.

An in-depth discussion of the possible formation scenarios for this binary system is beyond the scope of the paper; nevertheless, a few aspects ought to be highlighted. As discussed in El-Badry et al. (2023b,a), the formation of the *Gaia* BH1 and BH2 systems as isolated binaries is unlikely. This is also true for the recently discovered *Gaia* NS1 system (El-Badry et al. 2024), composed of a high-mass neutron star and a low-metallicity star. Given the size of their orbits, these systems should have experienced a common-envelope phase and then a mass transfer toward the light companion, which would then have resulted in much closer orbits than the observed ones. For *Gaia* BH2, the common-envelope phase could have been avoided if the BH progenitor was more massive than $65\ M_\odot$. In the case of *Gaia* BH3, the present-day minimum separation is of the order of $1000\ R_\odot$ and the common-envelope phase could not have been avoided because models predict that the BH progenitor becomes a red supergiant even at $150\ M_\odot$ (Chen et al. 2015). Similarly to *Gaia* BH1 and BH2, the chemical composition of the luminous component does not show any unusual abundance; in particular, the absence of ^{13}C and the observed [Ba/Fe] point toward a lack of contamination by the BH progenitor during its evolution. The observed enhanced Eu abundance could be due to the contamination from the SN at the birth of the BH, but also due to the medium in which the star formed. An alternative formation scenario, proposed to explain the *Gaia* BH1 and BH2 systems, is that the BH acquired the low-mass companion via dynamical exchange in a dense environment (see for example Rastello et al. 2023; Tanikawa et al. 2024). Such a scenario might be supported by the probable association of *Gaia* BH3 with the ED-2 stream, which could be a remnant of a globular cluster (Dodd et al. 2023; Balbinot et al. 2023).

4. Conclusions

In this Letter, we present the discovery of a wide binary composed of a very metal-poor giant orbiting a dark object of $33\ M_\odot$, using *Gaia* preliminary DR4 astrometric data, corroborated by *Gaia* spectroscopy. Most probably, the massive dark object is a single black hole (BH). The $33\ M_\odot$ of the BH mass makes it the most massive BH of stellar origin discovered in our Galaxy. All Galactic BHs that reside in short-period X-ray binaries have masses generally below $10\ M_\odot$ (e.g. Corral-Santana et al. 2016), except Cyg-X1 ($M_{\mathrm{BH}} \sim 20\ M_\odot$). Even the first two dormant BHs discovered by *Gaia* in wide astrometric orbits have masses of about $10\ M_\odot$. The mass of *Gaia* BH3 puts it in the mass range of the BHs discovered by gravitational waves (e.g. Abbott et al. 2023), and, in fact, it is close to the peak of the observed mass distribution for the merging BHs (e.g. Farah et al. 2024). The metallicity of the system supports the scenario (Belczynski et al. 2016) that the high-mass BHs observed by LIGO/Virgo/KAGRA are the remnants of metal-poor stars.

The discovered system, with its extremely low-mass ratio, wide orbit, and specific chemical composition, can also provide constraints for stellar evolution and binary models. As in the case of the *Gaia* BH1 and BH2 systems, the formation scenario as an isolated binary appears unlikely and alternative scenarios should be considered. The BHs discovered by *Gaia* in wide binaries in our Galaxy and those detected by LIGO/Virgo/KAGRA in external galaxies (i.e. BH merger events of extremely short-period binaries) constitute two ends of the BH population. When stud-

ied together, they can help to formulate a comprehensive view of BH formation and the evolution of their progenitors.

Finally, the bright magnitude of the system and its relatively small distance makes it an easy target for further observations and detailed analyses by the astronomical community. This discovery should be also seen as a preliminary teaser for the content of *Gaia* DR4, which will undoubtedly reveal other binary systems hosting a BH.

References

Abbott, B. P., Abbott, R., Abbott, T. D., et al. 2016, Phys. Rev. Lett., 116, 061102
Abbott, R., Abbott, T. D., Abraham, S., et al. 2021, ApJ, 913, L7
Abbott, R., Abbott, T. D., Abraham, S., et al. 2020, ApJ, 900, L13
Abbott, R., Abbott, T. D., Acernese, F., et al. 2023, Physical Review X, 13, 011048
Andrae, R., Fouesneau, M., Sordo, R., et al. 2023, A&A, 674, A27
Babusiaux, C., Fabricius, C., Khanna, S., et al. 2023, A&A, 674, A32
Balbinot, E., Helmi, A., Callingham, T., et al. 2023, A&A, 678, A115
Bavera, S. S., Fragos, T., Zapartas, E., et al. 2023, Nature Astronomy, 7, 1090
Beers, T. C. & Christlieb, N. 2005, ARA&A, 43, 531
Belczynski, K., Bulik, T., Fryer, C. L., et al. 2010a, ApJ, 714, 1217
Belczynski, K., Dominik, M., Bulik, T., et al. 2010b, ApJ, 715, L138
Belczynski, K., Holz, D. E., Bulik, T., & O'Shaughnessy, R. 2016, Nature, 534, 512
Belczynski, K., Taam, R. E., Kalogera, V., Rasio, F. A., & Bulik, T. 2007, ApJ, 662, 504
Bergemann, M., Collet, R., Amarsi, A. M., et al. 2017, ApJ, 847, 15
Bergemann, M., Lind, K., Collet, R., Magic, Z., & Asplund, M. 2012, MNRAS, 427, 27
Blomme, R., Edvardsson, B., Eriksson, K., et al. 2017, Synthetic spectra used by CU6 in DR2, Gaia Data Processing and Analysis Consortium (DPAC) technical note GAIA-C6-TN-ROB-RHB-005, http://www.cosmos.esa.int/web/gaia/public-dpac-documents
Bonifacio, P., Monaco, L., Salvadori, S., et al. 2021, A&A, 651, A79
Bovy, J. 2015, ApJS, 216, 29
Bressan, A., Marigo, P., Girardi, L., et al. 2012, MNRAS, 427, 127
Caffau, E., Ludwig, H. G., Steffen, M., Freytag, B., & Bonifacio, P. 2011, Sol. Phys., 268, 255
Carrasco, J. M., Weiler, M., Jordi, C., et al. 2021, A&A, 652, A86
Casagrande, L. & VandenBerg, D. A. 2014, MNRAS, 444, 392
Castelli, F. & Kurucz, R. L. 2003, in Modelling of Stellar Atmospheres, ed. N. Piskunov, W. W. Weiss, & D. F. Gray, Vol. 210, A20
Chakrabarti, S., Simon, J. D., Craig, P. A., et al. 2023, AJ, 166, 6
Chen, Y., Bressan, A., Girardi, L., et al. 2015, MNRAS, 452, 1068
Corral-Santana, J. M., Casares, J., Muñoz-Darias, T., et al. 2016, A&A, 587, A61
Creevey, O. L., Sordo, R., Pailler, F., et al. 2023, A&A, 674, A26
Cropper, M., Katz, D., Sartoretti, P., et al. 2018, A&A, 616, A5
De Angeli, F., Weiler, M., Montegriffo, P., et al. 2023, A&A, 674, A2

Dekker, H., D'Odorico, S., Kaufer, A., Delabre, B., & Kotzlowski, H. 2000, in Society of Photo-Optical Instrumentation Engineers (SPIE) Conference Series, Vol. 4008, Optical and IR Telescope Instrumentation and Detectors, ed. M. Iye & A. F. Moorwood, 534–545
Dodd, E., Callingham, T. M., Helmi, A., et al. 2023, A&A, 670, L2
El-Badry, K., Rix, H.-W., Cendes, Y., et al. 2023a, MNRAS, 521, 4323
El-Badry, K., Rix, H.-W., Quataert, E., et al. 2023b, MNRAS, 518, 1057
El-Badry, K., Simon, J. D., Reggiani, H., et al. 2024, arXiv e-prints, arXiv:2402.06722
Fabricius, C., Bastian, U., Portell, J., et al. 2016, A&A, 595, A3
Farah, A. M., Fishbach, M., & Holz, D. E. 2024, ApJ, 962, 69
Fitzpatrick, E. L., Massa, D., Gordon, K. D., Bohlin, R., & Clayton, G. C. 2019, ApJ, 886, 108
Fouesneau, M., Frémat, Y., Andrae, R., et al. 2023, A&A, 674, A28
Frebel, A., Casey, A. R., Jacobson, H. R., & Yu, Q. 2013, ApJ, 769, 57
Fryer, C. L., Belczynski, K., Wiktorowicz, G., et al. 2012, ApJ, 749, 91
Gaia Collaboration, Arenou, F., Babusiaux, C., et al. 2023a, A&A, 674, A34
Gaia Collaboration, Prusti, T., de Bruijne, J. H. J., et al. 2016, A&A, 595, A1
Gaia Collaboration, Vallenari, A., Brown, A. G. A., et al. 2023b, A&A, 674, A1
Halbwachs, J. L. 2009, MNRAS, 394, 1075
Halbwachs, J.-L., Pourbaix, D., Arenou, F., et al. 2023, A&A, 674, A9
Hayashi, T., Suto, Y., & Trani, A. A. 2023, ApJ, 958, 26
Holl, B., Fabricius, C., Portell, J., et al. 2023, A&A, 674, A25
Hurley, J. R., Pols, O. R., & Tout, C. A. 2000, MNRAS, 315, 543
Katz, D., Sartoretti, P., Guerrier, A., et al. 2023, A&A, 674, A5
Korotin, S. A., Andrievsky, S. M., Hansen, C. J., et al. 2015, A&A, 581, A70
Kovalev, M., Brinkmann, S., Bergemann, M., & MPIA IT-department. 2018, NLTE MPIA web server, Max Planck Institute for Astronomy, Heidelberg, http://nlte.mpia.de
Kurucz, R. L. 2005, Memorie della Societa Astronomica Italiana Supplementi, 8, 14
Lallement, R., Vergely, J. L., Babusiaux, C., & Cox, N. L. J. 2022, A&A, 661, A147
Lépine, S. & Shara, M. M. 2005, AJ, 129, 1483
Lindegren, L. & Bastian, U. 2022, Local plane coordinates for the detailed analysis of complex Gaia sources, Gaia Data Processing and Analysis Consortium (DPAC) technical note GAIA-C3-TN-LU-LL-061, http://www.cosmos.esa.int/web/gaia/public-dpac-documents
Lindegren, L., Bastian, U., Biermann, M., et al. 2021a, A&A, 649, A4
Lindegren, L., Klioner, S. A., Hernández, J., et al. 2021b, A&A, 649, A2
Lindegren, L., Lammers, U., Hobbs, D., et al. 2012, A&A, 538, A78
Lodders, K., Palme, H., & Gail, H. P. 2009, Landolt Börnstein, 4B, 712
Lombardo, L., François, P., Bonifacio, P., et al. 2021, A&A, 656, A155
Mashonkina, L., Korn, A. J., & Przybilla, N. 2007, A&A, 461, 261
McMillan, P. J. 2017, MNRAS, 465, 76
Miller-Jones, J. C. A., Bahramian, A., Orosz, J. A., et al. 2021, Science, 371, 1046
Montegriffo, P., De Angeli, F., Andrae, R., et al. 2023, A&A, 674, A3
Mucciarelli, A., Salaris, M., & Bonifacio, P. 2012, MNRAS, 419, 2195
Myeong, G. C., Vasiliev, E., Iorio, G., Evans, N. W., & Belokurov, V. 2019, MNRAS, 488, 1235
Nagarajan, P., El-Badry, K., Triaud, A. H. M. J., et al. 2024, PASP, 136, 014202
Olejak, A., Belczynski, K., Bulik, T., & Sobolewska, M. 2020, A&A, 638, A94
Perruchot, S., Kohler, D., Bouchy, F., et al. 2008, in Society of Photo-Optical Instrumentation Engineers (SPIE) Conference Series, Vol. 7014, Ground-based and Airborne Instrumentation for Astronomy II, ed. I. S. McLean & M. M. Casali, 70140J
Pietrinferni, A., Hidalgo, S., Cassisi, S., et al. 2021, ApJ, 908, 102
Pourbaix, D., Arenou, F., Gavras, P., et al. 2022, Gaia DR3 documentation Chapter 7: Non-Single Stars, Gaia DR3 documentation
Raskin, G., van Winckel, H., Hensberge, H., et al. 2011, A&A, 526, A69
Rastello, S., Iorio, G., Mapelli, M., et al. 2023, MNRAS, 526, 740
Recio-Blanco, A., de Laverny, P., Palicio, P. A., et al. 2023, A&A, 674, A29
Riello, M., De Angeli, F., Evans, D. W., et al. 2021, A&A, 649, A3
Sahlmann, J. 2019, Johannes-Sahlmann/pystrometry: Release for Zenodo, https://doi.org/10.5281/zenodo.3515526
Sahu, K. C., Anderson, J., Casertano, S., et al. 2022, ApJ, 933, 83
Salaris, M., Chieffi, A., & Straniero, O. 1993, ApJ, 414, 580
Sartoretti, P., Blomme, R., David, M., & Seabroke, G. 2022, Gaia DR3 documentation Chapter 6: Spectroscopy, Gaia DR3 documentation
Sartoretti, P., Katz, D., Cropper, M., et al. 2018, A&A, 616, A6
Sartoretti, P., Marchal, O., Babusiaux, C., et al. 2023, A&A, 674, A6
Sbordone, L., Caffau, E., Bonifacio, P., & Duffau, S. 2014, A&A, 564, A109
Sitnova, T. M., Yakovleva, S. A., Belyaev, A. K., & Mashonkina, L. I. 2022, MNRAS, 515, 1510
Sukhbold, T., Ertl, T., Woosley, S. E., Brown, J. M., & Janka, H. T. 2016, ApJ, 821, 38
Tanikawa, A., Cary, S., Shikauchi, M., Wang, L., & Fujii, M. S. 2024, MNRAS, 527, 4031
Tanikawa, A., Hattori, K., Kawanaka, N., et al. 2023, ApJ, 946, 79

Tantalo, R., Chiosi, C., & Bressan, A. 1998, A&A, 333, 419
Ulla, A., Creevey, O. L., Álvarez, M. A., et al. 2022, Gaia DR3 documentation
    Chapter 11: Astrophysical parameters, Gaia DR3 documentation
Vergely, J. L., Lallement, R., & Cox, N. L. J. 2022, A&A, 664, A174
Vink, J. S. 2008, New A Rev., 52, 419

[1] GEPI, Observatoire de Paris, Université PSL, CNRS, 5 Place Jules Janssen, 92190 Meudon, France

[2] School of Physics and Astronomy, Tel Aviv University, Tel Aviv 6997801, Israel

[3] Department of Astronomy, University of Geneva, Chemin Pegasi 51, 1290 Versoix, Switzerland

[4] Department of Astronomy, University of Geneva, Chemin d'Ecogia 16, 1290 Versoix, Switzerland

[5] Institut d'Astronomie et d'Astrophysique, Université Libre de Bruxelles CP 226, Boulevard du Triomphe, 1050 Brussels, Belgium

[6] Univ. Grenoble Alpes, CNRS, IPAG, 38000 Grenoble, France

[7] RHEA for European Space Agency (ESA), Camino bajo del Castillo, s/n, Urbanización Villafranca del Castillo, Villanueva de la Cañada, 28692 Madrid, Spain

[8] Astronomisches Rechen-Institut, Zentrum für Astronomie der Universität Heidelberg, Mönchhofstr. 12-14, 69120 Heidelberg, Germany

[9] Astronomical Observatory, University of Warsaw, Al. Ujazdowskie 4, 00-478 Warszawa, Poland

[10] HE Space Operations BV for European Space Agency (ESA), Camino bajo del Castillo, s/n, Urbanización Villafranca del Castillo, Villanueva de la Cañada, 28692 Madrid, Spain

[11] Mullard Space Science Laboratory, University College London, Holmbury St Mary, Dorking, Surrey RH5 6NT, United Kingdom

[12] Telespazio UK S.L. for European Space Agency (ESA), Camino bajo del Castillo, s/n, Urbanización Villafranca del Castillo, Villanueva de la Cañada, 28692 Madrid, Spain

[13] Kapteyn Astronomical Institute, University of Groningen, Landleven 12, 9747 AD Groningen, The Netherlands

[14] Leiden Observatory, Leiden University, Einsteinweg 55, 2333 CC Leiden, The Netherlands

[15] INAF - Osservatorio astronomico di Padova, Vicolo Osservatorio 5, 35122 Padova, Italy

[16] European Space Agency (ESA), European Space Research and Technology Centre (ESTEC), Keplerlaan 1, 2201AZ, Noordwijk, The Netherlands

[17] CNES Centre Spatial de Toulouse, 18 avenue Edouard Belin, 31401 Toulouse Cedex 9, France

[18] Université Côte d'Azur, Observatoire de la Côte d'Azur, CNRS, Laboratoire Lagrange, Bd de l'Observatoire, CS 34229, 06304 Nice Cedex 4, France

[19] Laboratoire d'astrophysique de Bordeaux, Univ. Bordeaux, CNRS, B18N, allée Geoffroy Saint-Hilaire, 33615 Pessac, France

[20] Institute of Astronomy, University of Cambridge, Madingley Road, Cambridge CB3 0HA, United Kingdom

[21] Aurora Technology for European Space Agency (ESA), Camino bajo del Castillo, s/n, Urbanización Villafranca del Castillo, Villanueva de la Cañada, 28692 Madrid, Spain

[22] Institut de Ciències del Cosmos (ICCUB), Universitat de Barcelona (UB), Martí i Franquès 1, 08028 Barcelona, Spain

[23] Institut d'Estudis Espacials de Catalunya (IEEC), c. Esteve Terradas 1, 08860 Castelldefels (Barcelona), Spain

[24] Lohrmann Observatory, Technische Universität Dresden, Mommsenstraße 13, 01062 Dresden, Germany

[25] European Space Agency (ESA), European Space Astronomy Centre (ESAC), Camino bajo del Castillo, s/n, Urbanización Villafranca del Castillo, Villanueva de la Cañada, 28692 Madrid, Spain

[26] Lund Observatory, Division of Astrophysics, Department of Physics, Lund University, Box 43, 22100 Lund, Sweden

[27] Departament de Física Quàntica i Astrofísica (FQA), Universitat de Barcelona (UB), c. Martí i Franquès 1, 08028 Barcelona, Spain

[28] Nicolaus Copernicus Astronomical Center, Polish Academy of Sciences, ul. Bartycka 18, 00-716 Warsaw, Poland

[29] Instituut voor Sterrenkunde, KU Leuven, Celestijnenlaan 200D, 3001 Leuven, Belgium

[30] Department of Astrophysics/IMAPP, Radboud University, P.O.Box 9010, 6500 GL Nijmegen, The Netherlands

[31] Max Planck Institute for Astronomy, Königstuhl 17, 69117 Heidelberg, Germany

[32] INAF - Osservatorio Astrofisico di Torino, via Osservatorio 20, 10025 Pino Torinese (TO), Italy

[33] European Space Agency (ESA, retired), European Space Research and Technology Centre (ESTEC), Keplerlaan 1, 2201AZ, Noordwijk, The Netherlands

[34] Royal Observatory of Belgium, Ringlaan 3, 1180 Brussels, Belgium

[35] DAPCOM Data Services, c. dels Vilabella, 5-7, 80500 Vic, Barcelona, Spain

[36] Observational Astrophysics, Division of Astronomy and Space Physics, Department of Physics and Astronomy, Uppsala University, Box 516, 751 20 Uppsala, Sweden

[37] Gaia DPAC Project Office, ESAC, Camino bajo del Castillo, s/n, Urbanización Villafranca del Castillo, Villanueva de la Cañada, 28692 Madrid, Spain

[38] SYRTE, Observatoire de Paris, Université PSL, CNRS, Sorbonne Université, LNE, 61 avenue de l'Observatoire 75014 Paris, France

[39] IMCCE, Observatoire de Paris, Université PSL, CNRS, Sorbonne Université, Univ. Lille, 77 av. Denfert-Rochereau, 75014 Paris, France

[40] INAF - Osservatorio di Astrofisica e Scienza dello Spazio di Bologna, via Piero Gobetti 93/3, 40129 Bologna, Italy

[41] Serco Gestión de Negocios for European Space Agency (ESA), Camino bajo del Castillo, s/n, Urbanización Villafranca del Castillo, Villanueva de la Cañada, 28692 Madrid, Spain

[42] Institut d'Astrophysique et de Géophysique, Université de Liège, 19c, Allée du 6 Août, B-4000 Liège, Belgium

[43] CRAAG - Centre de Recherche en Astronomie, Astrophysique et Géophysique, Route de l'Observatoire Bp 63 Bouzareah 16340 Algiers, Algeria

[44] Institute for Astronomy, University of Edinburgh, Royal Observatory, Blackford Hill, Edinburgh EH9 3HJ, United Kingdom

[45] INAF - Osservatorio Astrofisico di Arcetri, Largo Enrico Fermi 5, 50125 Firenze, Italy

[46] CIGUS CITIC - Department of Computer Science and Information Technologies, University of A Coruña, Campus de Elviña s/n, A Coruña, 15071, Spain

[47] Kavli Institute for Cosmology Cambridge, Institute of Astronomy, Madingley Road, Cambridge, CB3 0HA

[48] Department of Astrophysics, Astronomy and Mechanics, National and Kapodistrian University of Athens, Panepistimiopolis, Zografos, 15783 Athens, Greece

[49] Donald Bren School of Information and Computer Sciences, University of California, Irvine, CA 92697, USA

[50] CENTRA, Faculdade de Ciências, Universidade de Lisboa, Edif. C8, Campo Grande, 1749-016 Lisboa, Portugal

[51] INAF - Osservatorio Astrofisico di Catania, via S. Sofia 78, 95123 Catania, Italy

[52] Dipartimento di Fisica e Astronomia ""Ettore Majorana"", Università di Catania, Via S. Sofia 64, 95123 Catania, Italy

[53] Université de Strasbourg, CNRS, Observatoire astronomique de Strasbourg, UMR 7550, 11 rue de l'Université, 67000 Strasbourg, France

[54] Department of Physics, University of Helsinki, P.O. Box 64, 00014 Helsinki, Finland

[55] Finnish Geospatial Research Institute FGI, Vuorimiehentie 5, 02150 Espoo, Finland

[56] Space Science Data Center - ASI, Via del Politecnico SNC, 00133 Roma, Italy

[57] Institut UTINAM CNRS UMR6213, Université de Franche-Comté, OSU THETA Franche-Comté Bourgogne, Observatoire de Besançon, BP1615, 25010 Besançon Cedex, France

[58] HE Space Operations BV for European Space Agency (ESA), Keplerlaan 1, 2201AZ, Noordwijk, The Netherlands

59 Dpto. de Inteligencia Artificial, UNED, c/ Juan del Rosal 16, 28040 Madrid, Spain

60 Leibniz Institute for Astrophysics Potsdam (AIP), An der Sternwarte 16, 14482 Potsdam, Germany

61 Konkoly Observatory, HUN-REN Research Centre for Astronomy and Earth Sciences, MTA Centre of Excellence, 1121, Konkoly Thege Miklós út 15-17, Budapest, Hungary

62 Institute of Physics and Astronomy, ELTE Eötvös Loránd University, 1117, Pázmány Péter sétány 1A, Budapest, Hungary

63 University of Vienna, Department of Astrophysics, Türkenschanzstraße 17, A1180 Vienna, Austria

64 ATG Europe for European Space Agency (ESA), Camino bajo del Castillo, s/n, Urbanización Villafranca del Castillo, Villanueva de la Cañada, 28692 Madrid, Spain

65 INAF - Osservatorio Astronomico di Roma, Via Frascati 33, 00078 Monte Porzio Catone (Roma), Italy

66 Centre for Astrophysics Research, University of Hertfordshire, College Lane, AL10 9AB, Hatfield, United Kingdom

67 Quasar Science Resources for European Space Agency (ESA), Camino bajo del Castillo, s/n, Urbanización Villafranca del Castillo, Villanueva de la Cañada, 28692 Madrid, Spain

68 LASIGE, Faculdade de Ciências, Universidade de Lisboa, Edif. C6, Campo Grande, 1749-016 Lisboa, Portugal

69 School of Physics and Astronomy, University of Leicester, University Road, Leicester LE1 7RH, United Kingdom

70 Astrophysics Group, Cavendish Laboratory, University of Cambridge, JJ Thomson Avenue, Cambridge CB3 0HE, United Kingdom

71 Telespazio for CNES Centre Spatial de Toulouse, 18 avenue Edouard Belin, 31401 Toulouse Cedex 9, France

72 University of Turin, Department of Physics, Via Pietro Giuria 1, 10125 Torino, Italy

73 ALTEC S.p.a, Corso Marche, 79,10146 Torino, Italy

74 University of Maryland, College Park, MD, USA

75 EURIX S.r.l., Corso Vittorio Emanuele II 61, 10128, Torino, Italy

76 Porter School of the Environment and Earth Sciences, Tel Aviv University, Tel Aviv 6997801, Israel

77 Harvard-Smithsonian Center for Astrophysics, 60 Garden St., MS 15, Cambridge, MA 02138, USA

78 Laboratoire de Recherche en Neuroimagerie, University Hospital (CHUV) and University of Lausanne (UNIL), Lausanne, Switzerland

79 Sydney Institute for Astronomy, School of Physics, University of Sydney, NSW 2006, Australia

80 ARC Centre of Excellence for All Sky Astrophysics in 3 Dimensions (ASTRO 3D), Australia

81 ATOS for CNES Centre Spatial de Toulouse, 18 avenue Edouard Belin, 31401 Toulouse Cedex 9, France

82 Department of Physics and Astronomy G. Galilei, University of Padova, Vicolo dell'Osservatorio 3, 35122, Padova, Italy

83 LFCA/DAS,Universidad de Chile,CNRS,Casilla 36-D, Santiago, Chile

84 University of West Attica, Ag. Spyridonos Str., Egaleo, 12243 Athens, Greece

85 SISSA - Scuola Internazionale Superiore di Studi Avanzati, via Bonomea 265, 34136 Trieste, Italy

86 SII for CNES Centre Spatial de Toulouse, 18 avenue Edouard Belin, 31401 Toulouse Cedex 9, France

87 University of Turin, Department of Computer Sciences, Corso Svizzera 185, 10149 Torino, Italy

88 Dpto. de Matemática Aplicada y Ciencias de la Computación, Univ. de Cantabria, ETS Ingenieros de Caminos, Canales y Puertos, Avda. de los Castros s/n, 39005 Santander, Spain

89 Institut de Física d'Altes Energies (IFAE), The Barcelona Institute of Science and Technology, Campus UAB, 08193 Bellaterra (Barcelona), Spain

90 Port d'Informació Científica (PIC), Campus UAB, C. Albareda s/n, 08193 Bellaterra (Barcelona), Spain

91 Centro de Investigaciones Energéticas, Medioambientales y Tecnológicas (CIEMAT), Avenida Complutense 40, E-28040 Madrid, Spain

92 Thales Services for CNES Centre Spatial de Toulouse, 18 avenue Edouard Belin, 31401 Toulouse Cedex 9, France

93 TBC

94 LESIA, Observatoire de Paris, Université PSL, CNRS, Sorbonne Université, Université de Paris, 5 Place Jules Janssen, 92190 Meudon, France

95 University of Turin, Mathematical Department ""G.Peano"", Via Carlo Alberto 10, 10123 Torino, Italy

96 Institute of Physics, Ecole Polytechnique Fédérale de Lausanne (EPFL), Observatoire de Sauverny, 1290 Versoix, Switzerland

97 University of Antwerp, Onderzoeksgroep Toegepaste Wiskunde, Middelheimlaan 1, 2020 Antwerp, Belgium

98 INAF - Osservatorio Astronomico d'Abruzzo, Via Mentore Maggini, 64100 Teramo, Italy

99 APAVE EXPLOITATION for CNES Centre Spatial de Toulouse, 18 avenue Edouard Belin, 31401 Toulouse Cedex 9, France

100 Dpto. Física Teórica y del Cosmos, Universidad de Granada, 18071 Granada, Spain

101 The Center for Cosmology and Particle Physics, New York University, 726 Broadway New York, NY 10003, USA

102 NASA Hubble Fellow

103 Ruđer Bošković Institute, Bijenička cesta 54, 10000 Zagreb, Croatia

104 Finnish Centre for Astronomy with ESO, University of Turku, FI-20014 Turku, Finland

105 Astrophysics Research Centre, School of Mathematics and Physics, Queen's University Belfast, Belfast BT7 1NN, UK

106 Institute for Computational Cosmology, Department of Physics, Durham University, Durham DH1 3LE, UK

107 Data Science and Big Data Lab, Pablo de Olavide University, 41013, Seville, Spain

108 Institute of Astrophysics, FORTH, Crete, Greece

109 Barcelona Supercomputing Center (BSC), Plaça Eusebi Güell 1-3, 08034-Barcelona, Spain

110 Center for Astrophysics and Cosmology, University of Nova Gorica, Vipavska 13, 5000 Nova Gorica, Slovenia

111 F.R.S.-FNRS, Rue d'Egmont 5, 1000 Brussels, Belgium

112 Asteroid Engineering Laboratory, Luleå University of Technology, Box 848, 981 28 Kiruna, Sweden

113 Las Cumbres Observatory, 6740 Cortona Drive Suite 102, Goleta, CA 93117, USA

114 Université Rennes, CNRS, IPR (Institut de Physique de Rennes) - UMR 6251, 35000 Rennes, France

115 INAF - Osservatorio Astronomico di Capodimonte, Via Moiariello 16, 80131, Napoli, Italy

116 Shanghai Astronomical Observatory, Chinese Academy of Sciences, 80 Nandan Road, Shanghai 200030, People's Republic of China

117 University of Chinese Academy of Sciences, No.19(A) Yuquan Road, Shijingshan District, Beijing 100049, People's Republic of China

118 São Paulo State University, Grupo de Dinâmica Orbital e Planetologia, CEP 12516-410, Guaratinguetá, SP, Brazil

119 CIGUS CITIC, Department of Nautical Sciences and Marine Engineering, University of A Coruña, Paseo de Ronda 51, 15071, A Coruña, Spain

120 Astrophysics Research Institute, Liverpool John Moores University, 146 Brownlow Hill, Liverpool L3 5RF, United Kingdom

121 IRAP, Université de Toulouse, CNRS, UPS, CNES, 9 Av. colonel Roche, BP 44346, 31028 Toulouse Cedex 4, France

122 Serco Gestión de Negocios for European Space Agency (ESA), Camino bajo del Castillo, s/n, Urbanizacion Villafranca del Castillo, Villanueva de la Cañada, 28692 Madrid, Spain

123 Astronomical Institute, Faculty of Mathematics and Physics, Charles University, V Holešovičkách 2, 180 00 Prague, Czech Republic

[124] Dribia Data Research S.L., Pg. de Gràcia, 55, 3r 4a, 08007 Barcelona

[125] Pioneer Research Center for Climate and Earth Science, Institute for Basic Science, Daejeon 34126, Republic of Korea

[126] Astronomical Observatory, Jagiellonian University, ul. Orla 171, 30-244 Kraków, Poland

[127] Center for Computational Astrophysics, Flatiron Institute, 163 Fifth Ave, New York, NY 10010, USA

[128] INAF - Osservatorio Astronomico di Brera, via E. Bianchi, 46, 23807 Merate (LC), Italy

[129] National Astronomical Observatory of Japan, 2-21-1 Osawa, Mitaka, Tokyo 181-8588, Japan

[130] Department of Particle Physics and Astrophysics, Weizmann Institute of Science, Rehovot 7610001, Israel

[131] Centre de Données Astronomique de Strasbourg, Strasbourg, France

[132] University of Exeter, School of Physics and Astronomy, Stocker Road, Exeter, EX2 7SJ, United Kingdom

[133] Departamento de Astrofísica, Centro de Astrobiología (CSIC-INTA), ESA-ESAC. Camino Bajo del Castillo s/n. 28692 Villanueva de la Cañada, Madrid, Spain

[134] naXys, Department of Mathematics, University of Namur, Rue de Bruxelles 61, 5000 Namur, Belgium

[135] INAF. Osservatorio Astronomico di Trieste, via G.B. Tiepolo 11, 34131, Trieste, Italy

[136] H H Wills Physics Laboratory, University of Bristol, Tyndall Avenue, Bristol BS8 1TL, United Kingdom

[137] Instituto de Astronomia, Geofìsica e Ciências Atmosféricas, Universidade de São Paulo, Rua do Matão, 1226, Cidade Universitaria, 05508-900 São Paulo, SP, Brazil

[138] Escuela de Arquitectura y Politécnica - Universidad Europea de Valencia, Spain

[139] Escuela Superior de Ingeniería y Tecnología - Universidad Internacional de la Rioja, Spain

[140] Institut "ur Physik und Astronomie, Universit"at Potsdam, Haus 28, Karl-Liebknecht-Str. 24/25, 14476 Golm (Potsdam), Germany

[141] Applied Physics Department, Universidade de Vigo, 36310 Vigo, Spain

[142] Instituto de F'isica e Ciencias Aeroespaciais (IFCAE), Universidade de Vigo, Á Campus de As Lagoas, 32004 Ourense, Spain

[143] Purple Mountain Observatory and Key Laboratory of Radio Astronomy, Chinese Academy of Sciences, 10 Yuanhua Road, Nanjing 210033, People's Republic of China

[144] Sorbonne Université, CNRS, UMR7095, Institut d'Astrophysique de Paris, 98bis bd. Arago, 75014 Paris, France

[145] Faculty of Mathematics and Physics, University of Ljubljana, Jadranska ulica 19, 1000 Ljubljana, Slovenia

Appendix A: Astrometric processing in the NSS 4.1 run

Here, we provide the details of the Non-Single Star (NSS) pipeline used in the preliminary run NSS 4.1, underlining this is not the final version of the NSS pipeline for the generation of *Gaia* DR4 data.

The pipeline is similar to the one used in *Gaia* DR3 (Halbwachs et al. 2023), with a few updates – the main differences are in the improvement of the filters to remove spurious solutions. In particular, two new filters were introduced to remove sources which are partially resolved: the first one filters out sources with significant scan-angle-dependent signals (Holl et al. 2023) in the *G* flux before attempting an astrometric solution; the second one removes solutions which have periods that correspond to combinations of the *Gaia* spacecraft precession frequency and the yearly frequency (see Holl et al. 2023, Sect. 4.1). These new filters allow us to relax the filters based on the significance and on ϖ/σ_ϖ, described in Halbwachs et al. (2023), which are replaced by the following criteria: the goodness-of-fit (GoF) must be smaller than 15, the eccentricity error smaller than 0.2, semi-major axis significance $a_0/\sigma_{a_0} > 5$, and

$$\varpi/\sigma_\varpi > \max\left(15, -208.02 \cdot \log(P/1\,\mathrm{day}) + 548.03\right) . \quad (A.1)$$

The NSS 4.1 run was executed using astrometric data produced with preliminary runs (namely IDU 4.1 and AGIS 4.1) of the Intermediate Data Update (IDU; see Fabricius et al. 2016) and the Astrometric Global Iterative Solution (AGIS; see Lindegren et al. 2021b) pipelines. The preliminary astrometry provided by AGIS 4.1 covers the entire range of DR4, i.e. from JD 2456863.9385 to JD 2458869.4177, for a total of about 67 months, but only data after JD 2456941.6218 were used in the NSS 4.1 run. The local perspective effect (Halbwachs 2009) was not included in the model for the run NSS 4.1 and the variability-induced mover (VIM) solutions were not attempted.

The NSS 4.1 run was executed on a list of 10 450 939 sources chosen with the following criteria: the source must be brighter than $G_{\mathrm{RVS}} = 14$ mag and either $G < 18$ mag, an astrometric renormalised unit weight error (RUWE) larger than 1.05, or $\varpi > 5$ mas and RUWE > 0.9, and a number of visibility periods used in AGIS solution larger than 11. In order to exclude partially resolved sources, sources with a percent of successful Image Parameter Determination (IPD) windows with more than one peak larger than 10% or with amplitudes of the IPD GoF versus the scan angle larger than 0.2, were excluded (see *Gaia* DR3 archive documentation for details on the above quantities). The run produced a total of 1 469 196 orbital solutions.

The selection function of the NSS 4.1 run is not trivial to characterise, thus, it is not possible to estimate how common or rare are systems like *Gaia* BH3. If we push Gaia BH3 to the distance corresponding to the cut in magnitude ($G_{\mathrm{RVS}} = 14$ mag would correspond to a distance of 3.3 kpc, ignoring the extinction), the semi-major axis of the orbit would be 4.8 mas, which is still very large with respect to the precision of Gaia epoch measurements at that magnitude. However, given that the DR4 time range covers only half of the orbital period, the resulting significance could be below the acceptance thresholds. We note that during the *Gaia* DR3 preparation, *Gaia* BH3 produced an astrometric acceleration solution (Halbwachs et al. 2023) and an SB1 solution (Gosset et al. in prep.), which were both discarded from the release due to a low significance, because the orbital period was much longer than the *Gaia* DR3 time span and the periastron passage was not covered by the DR3 time range.

If we consider a Gaia BH3-like system but with an orbital period similar or shorter of the DR4 time range (i.e. below 2000 days), the significance would be always higher than the acceptance threshold solution, with the exception of very short (<20 day) periods. We note that the NSS 4.1 is limited to periods larger than 10 days. For binaries with shorter periods, the giant would almost fill its Roche lobe and the source would probably be detected as a X-ray source.

Although it has not yet been finalised, the input list for DR4 will be significantly larger than for NSS 4.1, probably built as the sum of a volume-limited sample and a $G < 18$ magnitude-limited sample, as indicated above, though without the $G_{\mathrm{RVS}} < 14$ mag criterion. The motivation for the dedicated NSS 4.1 run and the reason for the latter criterion was the analysis of the effect of a deviation of the astrometry from the assumed single-star model on the calibration of the spectroscopic instrument.

Appendix B: *Gaia* epoch data

Here, we describe the *Gaia* epoch astrometric data and epoch radial velocities used to produce the binary solution of *Gaia* BH3.

The astrometric measurements of *Gaia* BH3 are provided in Table B.1. They were produced from preliminary pipelines, provisional instrument models and calibrations; as a consequence they will not be identical (but still similar) to the corresponding data to be produced and published for this star with DR4. Furthermore, the final epoch astrometry table in DR4 will contain many additional details and quality diagnostics on the individual measurements. A full explanation of the epoch astrometry is beyond the scope of the present short appendix. We refer the reader to the Gaia Technical Document Lindegren & Bastian (2022) and to Lindegren et al. (2012).

Each *Gaia* epoch astrometry record in Table B.1 corresponds to a transit of the source on one of the CCDs of the AF instrument. The Table is arranged as follows. Col. 1: `transit_id`[5], a unique identifier assigned to each detected celestial light source as its image transits the *Gaia* focal plane; Col. 2: AF CCD strip; Col. 3: Barycentric time, in JD, corresponding to the middle of the 4.41-second CCD exposure time; Col. 4: Along-scan position of the photocentre, with its associated uncertainty, which corresponds to the longitude of the observed photocentre in a 2D tangential coordinate system having its origin at a reference equatorial position, and having the axis of its longitude coordinate oriented corresponding to the scanning direction; Col. 5: Parallax factor, namely, the quantity by which it is necessary to multiply the parallax in order to obtain the contribution to the along-scan position due to the orbit of the spacecraft with respect to the Solar System barycentre; Col. 6: Scan angle, which is the angle of the scanning direction with respect to local ICRS North; Col. 7: Outlier flag, indicating whether the measurement was considered as an outlier (flag = 1) by the NSS pipeline and filtered out, or not (flag = 0), when solving for the astrometric-spectroscopic combined solution.

The reference position (α_0, δ_0), in the sense of Lindegren & Bastian (2022), for *Gaia* BH3 is

$$\alpha_0 = 294\overset{\circ}{.}82784900557243 , \delta_0 = 14\overset{\circ}{.}930918410309376 , \quad (B.1)$$

while the reference time is J2017.5 (JD 2457936.875).

Epoch RVS radial velocities, reported in Table B.2, were produced with the final pipeline, but not finalised with the post-processing; their values or uncertainties may slightly differ from

---

[5] A decoder for the `transit_id` is available on-line at https://gaia.esac.esa.int/decoder/transitidDecoder.jsp

Table B.1. *Gaia* BH3 epoch astrometry.

transit_id	AF strip	Time [BJD, TCB]	Along-scan position [mas]	Parallax factor	Scan angle [deg]	Outlier flag
20114916805338633	1	2456958.110978	147.066 ± 0.370	0.70827985	−59.04672662	0
20114916805338633	2	2456958.111034	146.696 ± 0.231	0.70827991	−59.04677105	0
20114916805338633	3	2456958.111091	146.685 ± 0.183	0.70828003	−59.04681553	0
20114916805338633	4	2456958.111156	146.557 ± 0.151	0.70828015	−59.04686711	0
20114916805338633	5	2456958.111203	146.396 ± 0.097	0.70828021	−59.04690435	0
20114916805338633	6	2456958.111259	146.374 ± 0.088	0.70828027	−59.04694869	0
20114916805338633	7	2456958.111325	146.436 ± 0.100	0.70828038	−59.04700014	0
20114916805338633	8	2456958.111372	146.060 ± 0.100	0.70828044	−59.04703723	1
20114916805338633	9	2456958.111437	146.256 ± 0.130	0.70828056	−59.04708855	0
20119009095238725	1	2456958.184993	146.244 ± 0.364	0.70847327	−59.11055165	0
20119009095238725	2	2456958.185043	146.148 ± 0.296	0.70847344	−59.11059886	0
20119009095238725	3	2456958.185105	146.192 ± 0.267	0.70847368	−59.11065699	0
20119009095238725	4	2456958.185162	146.271 ± 0.225	0.70847386	−59.11070963	0
20119009095238725	5	2456958.185218	146.047 ± 0.273	0.70847410	−59.11076223	0
20119009095238725	6	2456958.185274	146.068 ± 0.158	0.70847428	−59.11081482	0
20119009095238725	7	2456958.185330	146.023 ± 0.177	0.70847452	−59.11086742	0
20119009095238725	8	2456958.185386	146.095 ± 0.191	0.70847470	−59.11092003	0
...	...	...	...	...	...	...

Notes. The full table is available at the CDS.

Table B.2. *Gaia* BH3 epoch radial velocities from *Gaia* RVS.

transit_id	Time [BJD, TCB]	Radial velocity [km s^{-1}]
22989619581449144	2457010.096166	−338.62 ± 1.42
22993711812243969	2457010.170169	−341.08 ± 1.70
27565894819405940	2457092.856649	−338.73 ± 1.41
27569987068420645	2457092.930660	−340.63 ± 1.43
29624665178404300	2457130.091203	−335.28 ± 2.20
37997278005744779	2457281.508798	−330.88 ± 1.24
52687653750370648	2457547.177378	−320.11 ± 1.61
60072325242450363	2457680.722202	−319.09 ± 1.87
61702852954182073	2457710.207118	−315.11 ± 1.12
68202800816349412	2457827.754668	−305.82 ± 1.53
81052816639971536	2458060.142534	−290.29 ± 1.42
82486181452083612	2458086.062277	−294.93 ± 1.53
82490273693622584	2458086.136278	−294.67 ± 1.75
100312802889225719	2458408.450948	−404.70 ± 1.14
111669627072959442	2458613.834346	−399.65 ± 1.21
112765863248582085	2458633.660613	−398.97 ± 1.10
121996985218154856	2458800.596176	−393.59 ± 2.00

Notes. The table is also available at the CDS.

the final DR4 values. As for the astrometry, the final epoch radial velocity table in DR4 will contain additional details and quality diagnostics on the individual measurements. Each epoch radial velocity record in Table B.2 corresponds to a transit of the source on the RVS CCDs. The provided observation time of the radial velocity corresponds to the mean of the observation times of the three CCDs used to collect spectra in the RVS during the transit.

A public code, illustrating the use of epoch astrometric and radial velocity data to produce an orbital solution for *Gaia* BH3 is available online[6].

---

[6] url to be determined

Appendix C: Ground-based spectroscopy

We observed *Gaia* BH3 with the HERMES spectrograph (Raskin et al. 2011) mounted on the 1.2-meter Mercator telescope at the Roque de los Muchachos Observatory (Spain), at two dates (17 July 2023 and 7 September 2023), taking two consecutive exposures of 2700 s each night. The spectra have a spectral coverage from 377 to 900 nm, a resolving power of 85 000, and a S/N ∼ 43 at 520 nm.

We observed *Gaia* BH3 also with the SOPHIE spectrograph (Perruchot et al. 2008) mounted on the 1.93-meter telescope of the Observatoire de Haute-Provence (France) on 4 September 2023. The source was observed with a single exposure of 6000 s; the spectra cover the range 387 to 694 nm with a resolving power of 40 000, and have a S/N ∼ 66 at 520 nm. HERMES and SO-PHIE spectra of *Gaia* BH3 are available on request from the corresponding author.

A search in the ESO archive revealed that the source was observed with the UVES spectrograph (Dekker et al. 2000) mounted on the VLT, on 5 November 2020, in the program 106.21JJ.001 proposed by T. Matsuno and collaborators. The aim of the program was to derive a complete chemical inventory of stars belonging to Galactic accretion events. The exposure time of the UVES spectrum was 900 s in the 390+580 setting (spectral coverage 326 to 454 nm and 476 to 684 nm) with a slit of 0.7″, producing a resolving power of 58 000 in the blue and 62 000 in the red and a S/N ∼ 100 at 520 nm.

For HERMES and SOPHIE observations, radial velocities were derived by computing the cross-correlation functions with a G2 mask, while for the UVES spectrum the radial velocity was derived via template matching. The barycentric radial-velocity values are reported in Table C.1, and they are in good agreement with the orbit derived from *Gaia* data. The spectra do not show any sign of the presence of a second component, nor any emission line. The UVES normalised spectrum of the *Gaia* BH3 in selected spectral regions is shown in Fig. C.1.
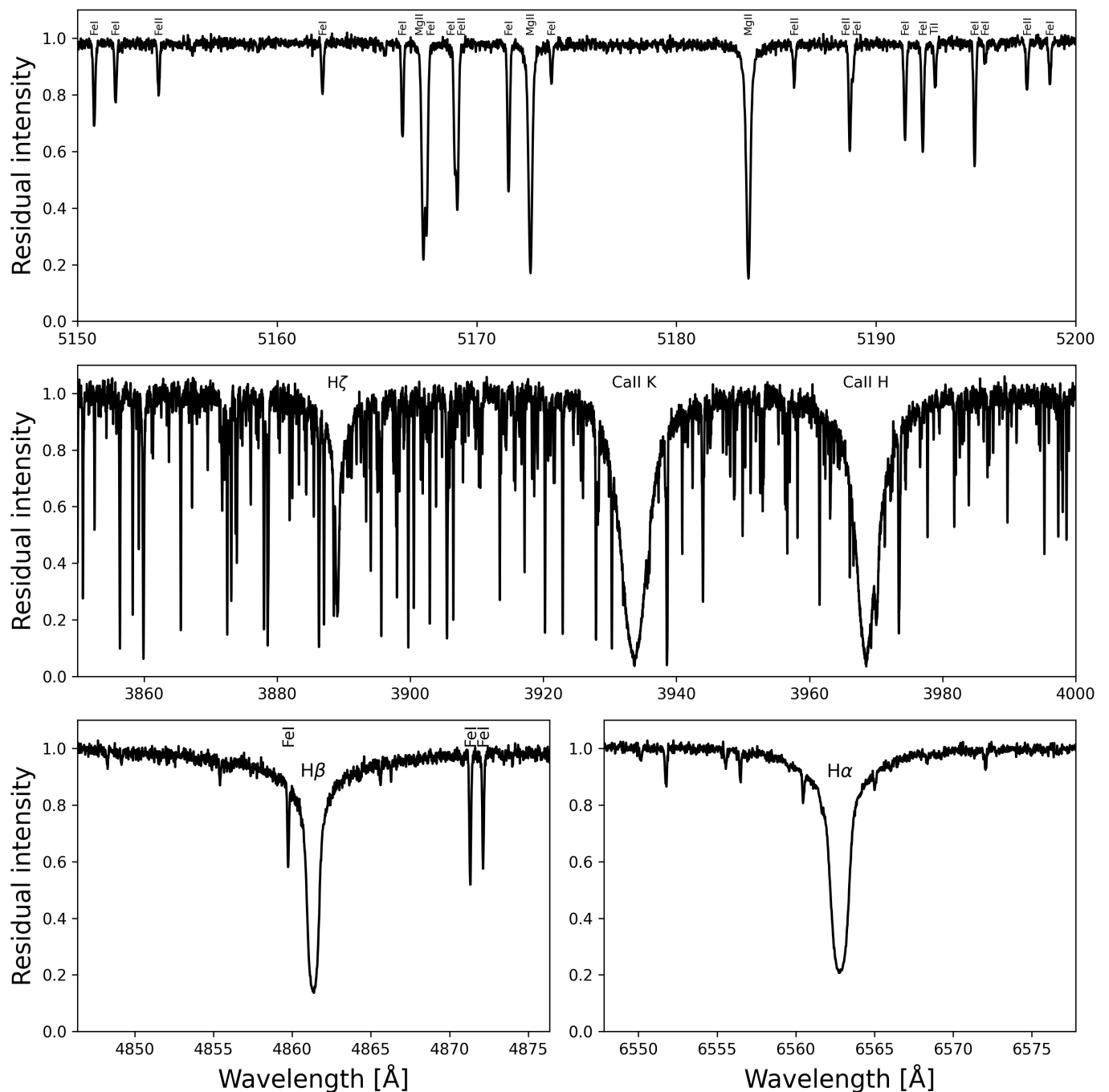
Fig. C.1. Residual intensity of the *Gaia* BH3 UVES spectrum in the magnesium triplet region (top panel), in the Ca ɪɪ H+K region (middle panel), Hβ (bottom-left) and Hα (bottom-right).

Table C.1. *Gaia* BH3 epoch radial velocities from ground-based observations.

Instrument	Time [BJD, UTC]	Radial velocity [km s^{-1}]
UVES	2459158.5333	-383.20 ± 0.30
HERMES	2460143.4948	-364.05 ± 0.20
SOPHIE	2460192.4359	-363.15 ± 0.02
HERMES	2460193.4833	-363.24 ± 0.20

Appendix D: Derivation of stellar parameters

Here we describe the iterative procedure used to derive the stellar parameters of the luminous component in *Gaia* BH3. The procedure is similar to the one adopted in Lombardo et al. (2021).

We computed the emerging flux for a grid in $T_{\rm eff}$, $\log g$ and [Fe/H], of 1D plane-parallel model atmospheres, using AT-LAS 9 (Castelli & Kurucz 2003; Kurucz 2005). The fluxes were then converted to spectral energy distributions by multiplying them by a factor $4\pi(R_\odot/10\,{\rm pc})^2$, where $R_\odot$ is the solar radius, as done in Casagrande & VandenBerg (2014). All models were computed assuming [α/Fe] = 0.4. For each model, we com-
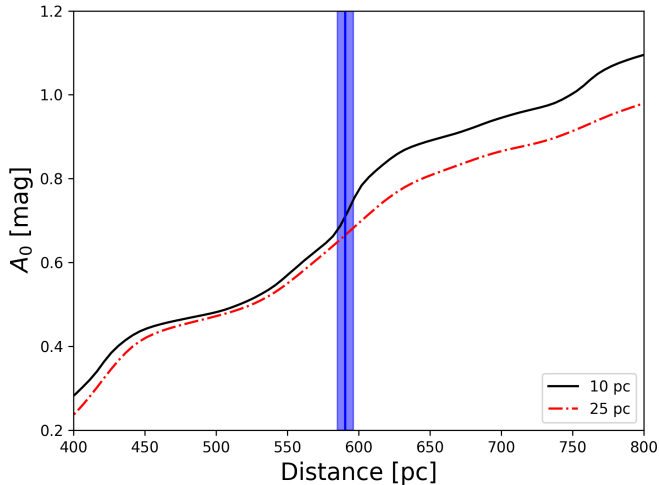
Fig. D.1. Extinction in the direction of *Gaia* BH3, as function of the distance. The extinction was derived with the maps with correlation length of 10 pc (black solid line) and 25 pc (red dot-dashed line) from Vergely et al. (2022); the vertical shaded region shows the distance range of *Gaia* BH3.
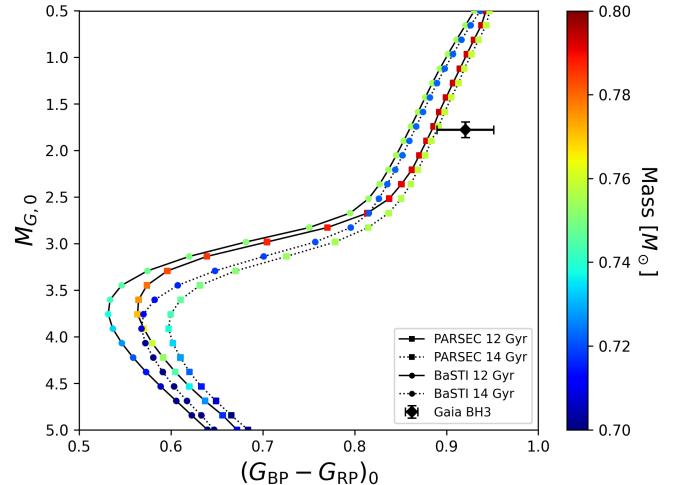

Fig. D.2. Comparison between the position of *Gaia* BH3 and isochrones in the colour-magnitude diagram. The colours of the symbols (filled circles for BaSTI and filled squares for PARSEC), on the two isochrones sets (12 and 14 Gyr), correspond to the stellar masses.

puted theoretical values of the color $G_{BP} - G_{RP}$, the bolometric correction (BC$_G$), and the extinction coefficients A_G/A_0 and $E(G_{BP} - G_{RP})/A_0$, using the average Milky Way reddening law from Fitzpatrick et al. (2019).

The iterative procedure starts with first-guess metallicity, temperature and gravity from *Gaia* DR3 values reported in Table 1, a first-guess mass ($M_\star$) of 0.8 $M_\odot$, and a given reddening of A_0. We use the above parameters to obtain $E(G_{BP} - G_{RP})$ from the grid, which is then used to obtain a dereddened $G_{BP} - G_{RP}$ colour, $(G_{BP} - G_{RP})_0$, the extinction A_G, and the bolometric correction BC$_G$. We then compare the $(G_{BP} - G_{RP})_0$ value to theoretical colours in the grid to derive a new effective temperature, and we use the Stefan-Boltzmann equation to derive a new surface gravity:

$$
\begin{aligned}
\log g = \ & \log \frac{M_\star}{M_\odot} + 4 \log \frac{T_{\text{eff}}}{T_\odot} + \log g_\odot + \hspace{2em} \text{(D.1)} \\
& + \ 0.4(G - A_G + BC_G - m_{\text{bol},\odot}) + 2 \log \frac{\varpi}{1000\,\text{mas}} \ .
\end{aligned}
$$

The procedure is repeated to convergence in T_{eff} and $\log g$ which is achieved after a few iterations. The parameters T_{eff} and $\log g$ are then used to derive the metallicity [Fe/H] as described in Sect. E and the process repeated.

The T_{eff}, $\log g$, and [Fe/H] derived with the above procedure depend mainly on the choice of A_0. *Gaia* BH3 has a low Galactic latitude ($b = -3.49°$), located in a zone with a relatively high gradient of A_0, according to extinction maps of Vergely et al. (2022), as can be seen in Fig. D.1. Adopting a distance of 590.6± 5.8 pc, we obtain $A_0 = 0.710^{+0.041}_{-0.034}$ mag for a correlation length of 10 pc and $A_0 = 0.666 \pm 0.017$ mag for a correlation length of 25 pc. We thus adopted $A_0 = 0.71 \pm 0.07$ mag.

An updated value for $M_\star$ can be then estimated by comparing the absolute G magnitude, $M_{G,0}$ and the colour $(G_{BP} - G_{RP})_0$ with the ones given by theoretical isochrones. The procedure for the determination of stellar parameters is finally repeated with the updated value of $M_\star$.

The value of $M_\star$ depends mainly on the assumed age and isochrone set, while it has a very small dependency on the as-

sumed A_0. We used isochrones from both PARSEC[7] (Bressan et al. 2012) and BaSTI[8] (Pietrinferni et al. 2021) libraries. For BaSTI, we adopt [Fe/H] = −2.5, [α/Fe] = 0.4 and [M/H] = −2.18, while for PARSEC isochrones, which are only available with no α-enhancement, we use metallicity [Fe/H] = −2.18, i.e. we scale the [Fe/H] to match the [M/H] of BaSTI isochrones and take into account the contribution of α-elements to the total metallicity (e.g. Salaris et al. 1993). The comparison between isochrones and *Gaia* BH3 in the $M_{G,0}$ versus $(G_{BP} - G_{RP})_0$ diagram is shown in Fig. D.2.

The value of $M_\star$ goes from 0.758 to 0.793 $M_\odot$ for PARSEC and 0.723 to 0.755 $M_\odot$ for BaSTI, for isochrone of ages 12 and 14 Gyr, respectively. Younger ages would result in higher masses, but also bluer colours. We then estimate a mass $M_\star = 0.76 \pm 0.05 M_\odot$ as the mass for the visible companion.

With the procedure described above, we obtain the following parameters: $T_{\text{eff}} = 5211 \pm 80$ K, $\log g = 2.929 \pm 0.003$, [Fe/H] = -2.56 ± 0.12. From the Mg I and Ca I abundances, we derived an α-enhancement of [α/Fe] = 0.43 ± 0.12. Using the relation between iron content, enhancement and metallicity from Tantalo et al. (1998), we obtain [M/H] = −2.21 ± 0.15.

It can be seen that the source is slightly redder and cooler than what is predicted by the models, albeit not significantly. In order to check that the T_{eff} that we determined above is not underestimated, we derived an alternative temperature estimation from the excitation equilibrium of the Fe I lines, including the NLTE corrections by Frebel et al. (2013). With this method, we obtained $T_{\text{eff}} \sim 5100$ K, which is even cooler, confirming that our estimation is not underestimated. A more detailed analysis of the stellar parameters is outside the scope of this work.

Appendix E: Abundances

We estimated the metallicity and abundances of the luminous component of *Gaia* BH3 from the UVES spectrum, which is of higher quality than our HERMES and SOPHIE spectra.

The abundances were derived with the code MyGIsFOS (Sbordone et al. 2014), with the exception of those for C, Ba

---

[7] http://stev.oapd.inaf.it/cgi-bin/cmd
[8] http://basti-iac.oa-abruzzo.inaf.it/isocs.html

and Eu; the carbon abundance was derived by fitting the Fraunhofer *G*-band of the CH molecule, while line-profile fitting was used to determine Ba and Eu abundances. The resulting values are listed in Table E.1. In the table, we provide the line-to-line scatter and the variation of the abundance corresponding to the uncertainty on the effective temperature. We adopted the solar abundances for C, Fe and Eu from Caffau et al. (2011), and those from Lodders et al. (2009) for the other elements. We derived a value of $1.19\,\mathrm{km\,s^{-1}}$ for the micro-turbulence, by forcing the same Fe abundance from Fe I lines of different equivalent width.

We sought the non-local thermal equilibrium (NLTE) correction for Mg I and Ca I in Kovalev et al. (2018). For the four Mg I lines available, we derived a NLTE correction of 0.06. Eleven lines of Ca I provided a NLTE correction of 0.15. The five Cr I lines available in the database provide a large NLTE correction: 0.46. For the Mn I features, the NLTE correction is 0.54. The 67 Fe I lines available provide a mean NLTE correction of 0.1. The NLTE effect on the Zn I line at 481 nm in Sitnova et al. (2022) and the Ba in Korotin et al. (2015) are small (see Table E.1).

The [Fe/H] ratio we derived from the UVES spectrum ([Fe/H] = −2.56 ± 0.12 from 223 Fe I lines) is in perfect agreement with the value derived from the SOPHIE spectrum ([Fe/H]= −2.57 ± 0.12 from 121 Fe I lines) and from the HERMES spectrum ([Fe/H]= −2.54 ± 0.14 from 156 Fe I lines). A good agreement was also obtained for the other elements, whose abundance is based on several lines. The star, as expected for the metal-poor regime, is enhanced in α elements.

There is no trace of ^{13}C in the spectrum, so the star has not been enriched by material processed in the CNO cycle, as it would if it had, for instance, accreted material from a companion star in the AGB phase.

The star has no chemical peculiarity, except a slight enhancement in Eu: [Eu/Fe] = 0.52. When coupled with [Ba/Fe] = 0.11, this classifies this star as an r-I neutron-capture-rich star, following the classification of Beers & Christlieb (2005). The UVES spectrum in the region of the Eu is shown in Fig. E.1.

According to the stellar parameters, the star is expected to have a Li abundance on the Mucciarelli plateau (see Mucciarelli et al. 2012). At the wavelength of the Li feature at 607 nm, we see an absorption line compatible with an abundance of A(Li) = 1.2, but the shape is not comparable with the synthetic spectrum, showing an absorption on the blue side of the feature. The Li feature is also visible in the SOPHIE spectrum, but with a lower S/N than in the UVES spectrum, while the S/N of the HERMES spectrum at 760 nm is too low.

Appendix F: Acknowledgements

Table E.1. Abundances of *Gaia* BH3 from UVES spectrum. The values A(X) are expressed in the form A(X) = log(X/H) + 12, while [X/H] = log (A(X)/A(X)$_\odot$).

Ion	N_{lines}	A(X)	[X/H]	$\sigma_{\mathrm{A(X)}}$ (1)	(2)	NLTE corr.
C I	...	6.11	-2.39	0.10	0.17	...
Mg I	5	5.46	-2.08	0.05	0.04	0.06^a
Ca I	20	4.13	-2.20	0.10	0.05	0.14^b
Sc II	6	0.76	-2.34	0.11	0.03	...
Ti I	17	2.67	-2.23	0.06	0.11	...
Ti II	26	2.80	-2.10	0.08	0.04	...
V I	3	1.34	-2.66	0.13	0.10	...
V II	6	1.61	-2.39	0.07	0.03	...
Cr I	5	2.86	-2.78	0.01	0.08	...
Cr II	3	3.23	-2.41	0.06	0.03	...
Mn I	7	2.45	-2.92	0.04	0.04	...
Mn II	1	2.79	-2.58	...	0.08	...
Fe I	223	4.96	-2.56	0.12	0.08	0.10^c
Fe II	15	5.03	-2.49	0.13	0.01	...
Co I	7	2.62	-2.30	0.09	0.11	...
Ni I	18	3.68	-2.55	0.12	0.06	...
Zn I	1	2.22	-2.40	...	0.02	0.12^d
Sr II	2	0.50	-2.42	0.05	0.08	...
Y II	10	-0.44	-2.65	0.16	0.05	...
Zr II	6	0.34	-2.28	0.12	0.05	...
Ba II	4	-0.28	-2.45	0.13	0.06	-0.10^e
La II	4	-1.22	-2.36	0.07	0.05	...
Eu II	1	-1.45	-1.97	...	0.05	...

Notes. The uncertainties on the abundances ($\sigma_{\mathrm{A(X)}}$) are reported as (1) line-to-line dispersion or (2) effect of T_{eff} uncertainty. NLTE corrections are from $^{(a)}$ Bergemann et al. (2017) , $^{(b)}$ Mashonkina et al. (2007) , $^{(c)}$ Bergemann et al. (2012) , $^{(d)}$ Sitnova et al. (2022) , $^{(e)}$ Korotin et al. (2015) .
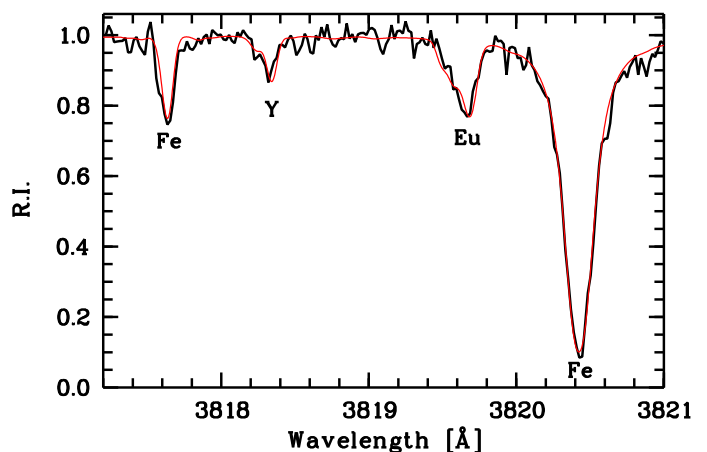

Fig. E.1. Residual intensity of the *Gaia* BH3 UVES spectrum (black line) compared with the modelled spectrum (thin red line) in the Eu region.